J Comput Aided Mol Des
DOI 10.1007/s10822-014-9820-5

Rational design of biaryl pharmacophore inserted noscapine derivatives as potent tubulin binding anticancer agents

Seneha Santoshi · Naresh Kumar Manchukonda · Charu Suri · Manya Sharma · Balasubramanian Sridhar · Silja Joseph · Manu Lopus · Srinivas Kantevari · Iswar Baitharu · Pradeep Kumar Naik

Received: 11 August 2014 / Accepted: 27 November 2014

Abstract We have strategically designed a series of noscapine derivatives by inserting biaryl pharmacophore (a major structural constituent of many of the microtubule-targeting natural anticancer compounds) onto the scaffold structure of noscapine. Molecular interaction of these derivatives with α,β-tubulin heterodimer was investigated by molecular docking, molecular dynamics simulation, and binding free energy calculation. The predictive binding affinity indicates that the newly designed noscapinoids bind to tubulin with a greater affinity. The predictive binding free energy ($\Delta G_{bind,\ pred}$) of these derivatives (ranging from −5.568 to −5.970 kcal/mol) based on linear interaction energy (LIE) method with a surface generalized Born (SGB) continuum solvation model showed improved binding affinity with tubulin compared to the lead compound, natural α-noscapine (−5.505 kcal/mol). Guided by the computational findings, these new biaryl type α-noscapine congeners were synthesized from 9-bromo-α-noscapine using optimized Suzuki reaction conditions for further experimental evaluation. The derivatives showed improved inhibition of the proliferation of human breast cancer cells (MCF-7), human cervical cancer cells (HeLa) and human lung adenocarcinoma cells (A549), compared to natural noscapine. The cell cycle analysis in MCF-7 further revealed that these compounds alter the cell cycle profile and cause mitotic arrest at G2/M phase more strongly than noscapine. Tubulin binding assay revealed higher binding affinity to tubulin, as suggested by dissociation constant (K_d) of 126 ± 5.0 μM for **5a**, 107 ± 5.0 μM for **5c**, 70 ± 4.0 μM for **5d**, and 68 ± 6.0 μM for **5e** compared to noscapine (K_d of 152 ± 1.0 μM). In fact, the experimentally determined value of $\Delta G_{bind,\ expt}$ (calculated from the K_d value) are consistent with the predicted value of $\Delta G_{bind,\ pred}$ calculated based on LIE–SGB. Based on these results, one of the derivative **5e** of this series was used for further toxicological evaluation. Treatment of mice with a daily dose of 300 mg/kg and a single dose of 600 mg/kg indicates that the compound does not induce detectable pathological abnormalities in normal tissues. Also there were no significant differences in hematological parameters between the treated and untreated groups. Hence, the newly designed noscapinoid, **5e** is an orally bioavailable, safe and effective anticancer agent with a potential for the treatment of cancer and might be a candidate for clinical evaluation.

S. Santoshi · C. Suri · M. Sharma · P. K. Naik (✉)
Department of Biotechnology and Bioinformatics, Jaypee University of Information Technology,
Waknaghat, Distt. Solan 173 234, Himachal Pradesh, India
e-mail: pknaik1973@gmail.com; pradeep.naik@juit.ac.in

N. K. Manchukonda · S. Kantevari
Organic Chemistry Division-II (CPC Division), CSIR-Indian Institute of Chemical Technology, Hyderabad 500 007, India
e-mail: kantevari@yahoo.com; kantevari@gmail.com

B. Sridhar
X-ray Crystallography Laboratory, CSIR-Indian Institute of Chemical Technology, Hyderabad 500 007, India

S. Joseph · M. Lopus
Experimental Cancer Therapeutics and Chemical Biology, Department of Biology, UM-DAE Centre for Excellence in Basic Sciences, University of Mumbai, Kalina, Santa Cruz (E), Mumbai 400 098, India

I. Baitharu
Department of Zoology, Guru Ghasidas Vishwavidyalaya (A Central University), Koni, Bilaspur 495 009, Chhattisgarh, India

Present Address:
P. K. Naik
Department of Biotechnology, Guru Ghasidas Vishwavidyalaya (A Central University), Koni, Bilaspur 495 009, Chhattisgarh, India

Published online: 07 December 2014

Keywords Noscapine · Noscapinoid · Tubulin · Molecular docking · Molecular dynamics simulation · Binding energy · Anticancer activity · Toxicity

Introduction

The crucial role that microtubules play in cell division makes them a suitable target for the development of chemotherapeutic drugs against the rapidly dividing cancer cells. This has been demonstrated by the clinical success of several vinca alkaloids (that depolymerize and decrease polymer mass of microtubules) and taxanes (that polymerize and bundle microtubules) [1, 2] in treating a variety of human cancers. However, their clinical success has been limited by the emergence of drug resistance as well as undesirable toxicities such as gastrointestinal effects (diarrhea, nausea, vomiting), myelosuppression (leucopenia), alopecia and peripheral neuropathies due to the blockage of axonal transport [3–5]. Besides, their high lipophilicity demands use of co-solvents like cremophor, which are associated with undesirable side effects. These shortcomings have prompted the search for novel microtubule-targeting compounds that display favorable toxicity profiles, have better therapeutic indices and superior pharmacological profiles.

It is crucial that microtubule dynamics must be aptly regulated for error-free progression of the cell cycle through mitosis. As a result, the compounds that either accelerate or suppress microtubule dynamics are correlated with impaired mitotic spindle function and inhibition of cell proliferation [6]. Previously, it has been demonstrated that noscapine and its derivatives (noscapinoids) suppress the dynamic instability of microtubule, thereby block cell cycle progression at mitosis, followed by apoptotic cell death in a wide variety of cancer cell types [7–10]. Furthermore, it has been observed that noscapine and one of its derivative (EM011, 9-bromo-noscapine) regress human xenografts of lymphomas, melanoma and breast tumors implanted in nude mice with little or no toxicity to the kidney, heart, liver, bone marrow, spleen, or small intestine, and do not inhibit primary humoral immune responses in mice [7, 11–13]. In addition, the water solubility, and feasibility for oral administration, also represent valuable advantages of noscapine over many other antimicrotubule drugs [14–16]. Hence, among the various antimitotic agents that perturb microtubule dynamics, noscapinoids constitute an emerging class of compounds receiving considerable attention. In our attempt to improve the therapeutic activity of noscapine, we have recently designed several noscapine analogues with better therapeutic indices [17–20].

However, it may be noted that compounds such as colchicine also perturbs the assembly dynamics of microtubules by interacting with tubulin, and remained as a useful lead candidate for generation of anticancer agents. However, due to toxic side effects, the use of colchicine as an anticancer agent is limited. Recent reports examined several natural and synthetic compounds such as Steganacin, Eupomatilone, Bufalvin, Wuwezi B and C, α-DDB, Bicyclol (Fig. 1) with colchicine like architecture and were found to possess potential anticancer activity. The observed anticancer activity was attributed to the pharmacophoric biaryl like structural features. Previously this pharmacophore feature has been used to synthesize biaryl based anticancer agents to act as antitumor agents with inhibition of tubulin assembly [21, 22]. With these observations, we envisaged that embedding the biaryl pharmacophore onto the natural noscapine could lead to new hybrid analogues.

As a proof of concept, in this study we computationally designed six derivatives of noscapine (Fig. 2) by inserting biaryl pharmacophore onto the scaffold structure of noscapine. Their binding affinity with tubulin was evaluated by means of molecular dynamics simulation followed by rescoring using MM-PBSA (molecular mechanics Poisson Boltzmann surface area) and MM-GBSA (molecular mechanics generalized Born surface area). All the designed noscapine analogues showed good predictive binding affinity with tubulin. Inspired from the molecular modeling calculations, we have synthesized these new derivatives from 9-bromo-noscapine by exploring optimized Suzuki reaction conditions and evaluated their biological activity. These new derivatives exhibited higher binding affinity for tubulin as evidenced by tryptophan quenching assay compared to the lead molecule, noscapine, and significantly inhibited proliferation of cancer cells. They displayed much lower IC_{50} values in comparison to noscapine in the three human cancer cell lines (MCF-7, a breast epithelial cancer cell line; HeLa, a cervix cell line and A549, a lung cancer cell line). The precise mechanism of action of these compounds involved a selective arrest of cell cycle progression at the G2/M phase in rapidly dividing cancer cells. Further, toxicity evaluation of one of the representative compounds from this series with mice revealed no evidence of toxicity. Our results indicate that the biaryl pharmacophore inserted noscapine derivatives are potential candidates for clinical evaluation.

Materials and methods

Molecular modeling

Computational design of noscapine derivatives and structure optimization

Molecular structures of the newly designed noscapine derivatives **5a–5f** (Fig. 2) as well as the previously

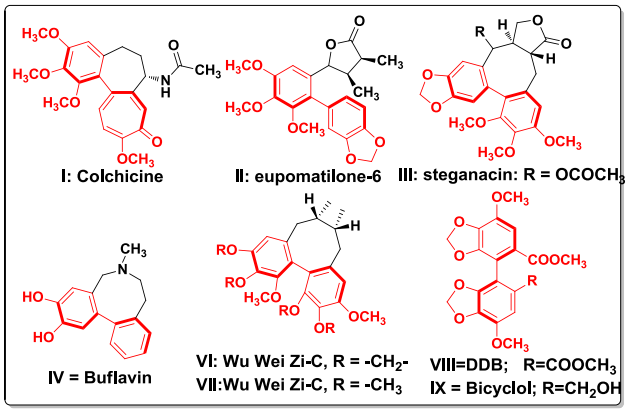

Fig. 1 Natural and synthetic analogues that are acting as microtubule targeting agents consist of biaryl (*red*) pharmacophore as major structural constituent. This pharmacophore feature is crucial for their biological activity

reported derivatives (used as training set, Fig. 3) were built using molecular builder of Maestro (version 9.2, Schrödinger). All these structures were energy minimized using Macromodel (version 9.9, Schrödinger) and OPLS 2005 force field with PRCG algorithm (1,000 steps of minimization and energy gradient of 0.001). Each structure was assigned an appropriate bond order using Ligprep (version 2.5, Schrödinger, LLC). Complete geometrical optimization of these structures was carried out using hybrid density functional theory (DFT) with Becke's three-parameter exchange potential and the Lee–Yang–Parr (B3LYP) correlation functional [23, 24] and using basis set 3-21G* [25]. Jaguar (version 7.7, Schrödinger, LLC) was used for the geometrical optimization of the ligands.

Protein preparation

The X-ray crystallographic structure of colchicine–tubulin complex (PDB ID: 1SA0, resolution 3.58 Å) was used for molecular docking of noscapine derivatives. This low resolution crystal structure was further refined as reported earlier [20]. Briefly, missing hydrogen atoms to the structure were added using Maestro (version 9.2, Schrödinger) and the hydrogen bond network of the complex was optimized using multi-step Schrödinger's protein preparation wizard (PPrep). The missing amino acids in the crystal structure were filled using Prime (version 3.0, Schrödinger). Furthermore, all atoms molecular dynamic (MD) simulation of protein structure in explicit water was carried out using GROMACS 4.5 [26] and AMBER99SB force field for 10 ns to refine the protein structure. A total of

Fig. 2 Molecular structure of newly designed noscapinoids, **5a**–**5f**. These molecules are rationally designed by substituting biaryl pharmacophore from the natural and synthetic analogues that are acting as microtubule targeting agents onto the scaffold structure of noscapine

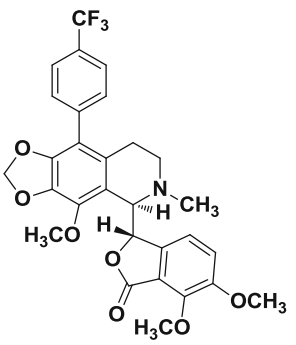

$(C_{29}H_{26}F_3NO_7)$, 5a

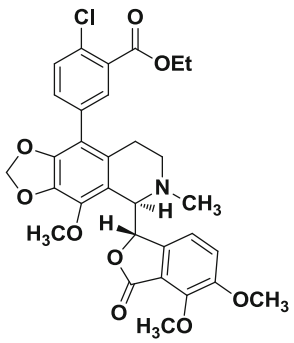

$(C_{31}H_{30}ClNO_9)$, 5b

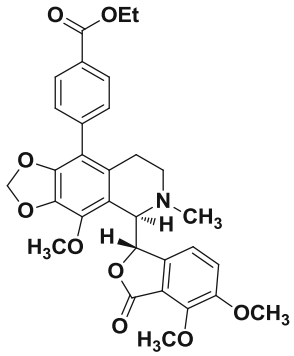

$(C_{31}H_{31}NO_9)$, 5c

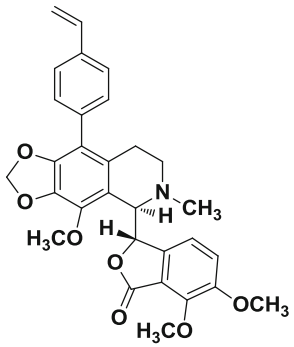

$(C_{30}H_{29}NO_7)$, 5d

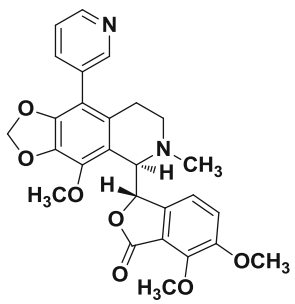

$(C_{27}H_{26}N_2O_7)$, 5e

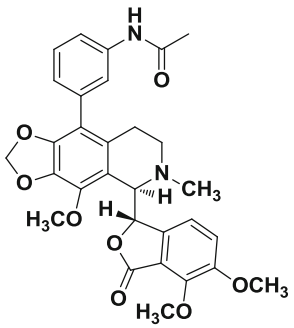

$(C_{30}H_{30}N_2O_8)$, 5f

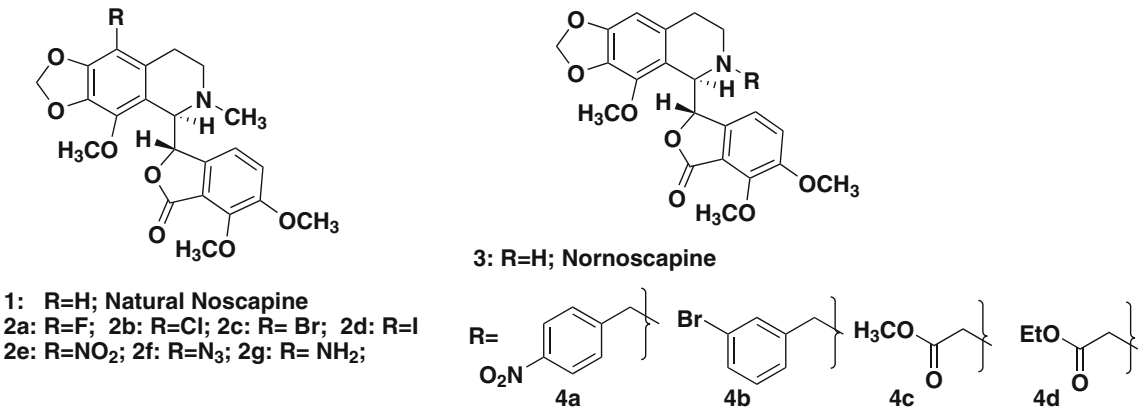

Fig. 3 Molecular structure of previously reported noscapinoids used in the training set

5,000 frames were generated in the MD trajectories, out of which the last 2,000 frames were used to generate an average structure of the tubulin. The overall quality of the model, stereochemical values and non-bonded interactions were evaluated using PROCHECK [27], ERRAT [28] and VERIFY3D [29]. The PROCHECK results showed 94.8 % of backbone angles were in allowed regions with G-factors of −0.12. Ramachandran et al. [30] plot analysis revealed only 1.6 % residues in the disallowed region and 2.3 % residues in generously allowed regions. The ERRAT score was 88.402 that is within the range of high quality model. Similarly, the VERIFY3D score of 95.25 % indicates a good quality model.

Molecular docking

The receptor-grid file was generated at the centroid of the noscapinoid binding site [31] using Glide (version 5.7, Schrödinger). A bounding box of size 12 Å × 12 Å × 12 Å was defined in tubulin and centered on the mass center of binding site in order to confine the mass center of the docked ligand. The larger enclosing box of size 12 Å × 12 Å × 12 Å which occupied all the atoms of the docked poses was also defined. The scale factor of 0.4 for van der Waals radii was applied to atoms of protein with absolute partial charges ≤0.25. All the ligands were then docked into the binding site using Glide XP (extra precision) and evaluated using a Glide XP_{Score} function [32, 33].

Molecular dynamics simulations

The best docked complexes of each compound, **5a**–**5f** with tubulin were used as initial conformation for MD simulation. The MD simulation was performed with the AMBER 11.0 software suite [34] using AMBER99SB force field [35]. Each molecular system was solvated with ~32,300 TIP3P water molecules in a truncated octahedral box and neutralized by adding 32 Na^+ ions. The molecular system was energy minimized in three consecutive rounds, each of which consisted of 500 steps of steepest descent followed by 500 steps of conjugate gradient energy minimization method so as to remove the bad contacts in the structure. With the force constants of 10 and 2 $kcal^{-1}$ $Å^{-2}$ respectively, positional restraints were applied to the whole system for the first and second round, to allow for relaxation of the solvent molecules. In the third round the whole system was minimized without restraint. Finally, a 10 ns MD simulation was carried out with a time step of 2 fs following 200 ps of equilibration at 300 K. SHAKE algorithm [36] was applied for all the bonds involving hydrogen bonds. The non bonded cut off distance was 10 Å, and the particle mesh ewald (PME) method [37] was applied to treat long-range electrostatic interactions. The temperature of the system was regulated using the langevin thermostat. All equilibration and subsequent MD stages were carried out in an isothermal isobaric (NPT) ensemble using Berendsen barometer [38, 39] with a target pressure of one bar and trajectories was recorded every 1 ps.

*Binding energy calculation of **5a**–**5f** with tubulin using MM-PBSA and MM-GBSA*

Binding energy of newly designed compounds, **5a**–**5f** with tubulin was calculated based on both MM-PBSA and MM-GBSA [40, 41] using AMBER 11.0. For this calculation, a total of 1,000 snapshots generated from the last 2 ns of the MD trajectory for each molecular species were considered. The binding energy (ΔG_{bind}) of the molecular species for each frame was then calculated as the difference between the energy of complex with the combination energy of receptor and ligand as follows.

$$\Delta G_{bind} = G_{complex} - (G_{receptor} + G_{ligand})$$

The free energy, G for each species was calculated as described previously using the MM-PBSA and MM-GBSA methods.

$$G = E_{gas} + G_{sol} - TS$$
$$E_{gas} = E_{int} + E_{ele} + E_{vdw}$$
$$G_{ele,PB(GB)} = E_{ele} + G_{PB(GB)}$$
$$G_{sol} = G_{sol-np} + G_{PB(GB)}$$
$$G_{sol-np} = \gamma SAS$$

Here, E_{gas} is the gas-phase energy; E_{int} is the internal energy; E_{ele} and E_{vdw} are the Coulomb and van der Waals energies, respectively. E_{gas} was calculated using the AMBER ff99SB molecular mechanics force field. G_{sol} is the solvation free energy which is decomposed into polar and non-polar contributions. $G_{PB(GB)}$ is the polar solvation contribution calculated by solving the PB and GB equations. $G_{ele,\ PB(GB)}$ is the polar interaction contribution. $G_{sol\text{-}np}$ is the non-polar solvation contribution and was estimated via the solvent-accessible surface area (SAS), which was determined using a water probe radius of 1.4 Å. T and S are the temperature and the total solute entropy, respectively.

Ligand-residue interaction decomposition

The binding energy contribution of each residue with the noscapinoids **5a–5f** within the binding cavity of α- and β-tubulin dimer was analyzed using MM-GBSA decomposition process utilizing MM-GBSA module in Amber 11.0. The binding energy of each ligand-residue pair includes three energy terms: the van der Waals contribution (ΔE_{vdw}), the electrostatic contribution (ΔE_{ele}) and the solvation contribution (ΔE_{sol}). All the energy components are calculated using the same frames obtained from MD trajectories that were used for calculation of binding energy of ligands.

*Predictive binding free energies of **5a–5f** towards tubulin using LIE–SGB method*

The predictive binding free energy ($\Delta G_{bind,\ pred}$) of the newly designed noscapinoids **5a–5f** with tubulin was determined using linear interaction energy model (LIE) with a surface generalized born (SGB) continuum solvation model proposed by Jorgensen [42] based on the experimental $\Delta G_{bind,\ expt}$ data of a set of training set molecules (Fig. 3). Liaison package (version 5.6, Schrödinger, LLC) was used to estimate the binding free energy based on empirical scoring function:

$$\Delta G_{bind,pred} = \alpha\left(\langle U^b_{vdw}\rangle - \left\langle U^f_{vdw}\right\rangle\right) + \beta\left(\langle U^b_{elec}\rangle - \left\langle U^f_{elec}\right\rangle\right) + \gamma\left(\langle U^b_{cav}\rangle - \langle U^f_{cav}\rangle\right) \quad (1)$$

Here $\langle\ \rangle$ represents the ensemble average, *b* represents the bound form of the ligand, *f* represents the free form of the ligand, and α, β, and γ are the coefficients. U_{vdw}, U_{elec}, and U_{cav} are the van der Waals, electrostatic, and cavity energy terms in the SGB continuum solvent model. The cavity energy term, U_{cav}, is proportional to the exposed surface area of the ligand. Various energy parameters included in Eq. 1 were calculated from the best docked complexes of these ligands by energy minimization based on Hybrid Monte Carlo simulation and Truncated Newton sampling technique using the OPLS-2005 force field. The system was initially heated to 300 K with a relaxation time of 15 ps. A residue-based cut off of 12 Å was set for the non-bonding interactions. With a maximum of 100 steps of minimization, the system was heated for 10 ps and finally Hybrid Monte Carlo simulation was performed for 15 ps. The α, β, and γ LIE fitting parameters were determined using Minitab statistical package (version 14.0, Minitab Inc.) by fitting the experimental binding affinities of training set molecules.

The experimental free energy of binding for the reported noscapinoids was calculated from their respective dissociation constant (K_d) values using the relation:

$$\Delta G_{bind} = RT \ln K_d$$

where R is gaseous constant (0.001986 kcal/mol) and T is temperature (298 K). The K_d values of the noscapinoids used in training set were obtained from earlier published work [18, 20, 43, 44] by measuring concentration dependent tubulin-binding curves derived from escalating concentrations of the compounds followed by Schatchard plots.

Chemistry

Chemical synthesis of noscapinoids

All the chemical reactions were carried out in oven-dried flasks with magnetic stirring. All the reagents and solvents used were of analytically grade. The progression of experiments was monitored by analytical thin layer chromatography (TLC) performed on silica gel GF254 pre-coated plates. The TLC plates after elution were visualized under UV illumination at 254 nm for UV active materials. Non-UV active materials were visualized by staining with PMA and charring on a hot plate. Silica gel finer than 200 mesh was used for column chromatography. Columns were packed as slurry of silica gel in hexane and equilibrated with the appropriate solvent/solvent mixture prior to use. The compounds were loaded neat or as a concentrated solution using the appropriate solvent system. Yields refer to chromatographically and spectroscopically homogeneous materials,

unless otherwise stated. Appropriate names for all the new compounds were given with the help of ChemBioOffice 2012. Melting points were measured with a Fischer-Johns melting point apparatus and were uncorrected. Infrared spectroscopy (IR) spectra were recorded as neat liquids or KBr pellets and absorptions were reported in cm^{-1}. Optical rotations were measured with a Roudolph Digipol 781 Polarimeter at 25 °C. Nuclear magnetic resonance (NMR) spectra were recorded on 300 (Bruker) and 500 MHz (Varian) spectrometers in appropriate solvents using tetramethylsilane (TMS) as an internal standard or the solvent signals as secondary standards and the chemical shifts are shown in δ scales. Multiplicities of NMR signals are designated as s (singlet), d (doublet), t (triplet), q (quartet), br (broad), m (multiplet, for unresolved lines), etc. ^{13}C NMR spectra were recorded on 75 MHz spectrometer. High-resolution mass spectra (HRMS) were obtained by using ESI-QTOF mass spectrometry. Purity of all the compounds (>96 %) used for biological screening were determined by analytical HPLC (SPD-M20A, make: Shimadzu) using ODS column eluted with gradient mixture of acetonitrile–water. Natural α-noscapine was purchased from Sigma-Aldrich and is used as such. The synthetic approach for the preparation of newly designed noscapine derivatives, **5a**–**5f** is depicted in Fig. 4.

*General procedure for the preparation of 9-arylnoscapines **5a**–**5f***

In an oven dried round bottom flask, 9-bromonoscapine (0.2 g, 0.4072 mmol) in ethanol, toluene (10 mL, v/v, 1:1), aryl boronic acids **6a**–**6f** (Fig. 5) (0.8145 mmol), $Pd(PPh_3)_4$ (0.04886 mmol) and sodium bicarbonate (0.8145 mmol) were added and heated at 120 °C for 48 h. The reaction mixture was cooled to room temperature, solvents were removed under reduced pressure, water (10 mL) was added to the crude residue, then extracted with dichloromethane (3 × 25 mL), and combined organic portion was dried over anhydrous sodium sulphate and evaporated. The crude product was purified over silica gel column chromatography (25 % EtOAc in Hexanes) to give pure compounds **5a**–**5f** as white solids.

*(S)-6,7-Dimethoxy-3-((R)-4-methoxy-6-methyl-9-(4-(trifluoromethyl)phenyl)-5,6,7,8-tetrahydro-[1,3]dioxolo[4,5-g]isoquinolin-5-yl)isobenzofuran-1(3H)-one (**5a**)* Yield: 65 %; m.p: 135 °C; $[\alpha]_D^{25}$: −62.22 ($c = 1$, dichloromethane); ^1H NMR ($CDCl_3$, 300 MHz) δ 7.60–7.40 (m, 4H), 6.97 (d, $J = 8.1$ Hz, 1H), 6.05 (d, $J = 8.3$ Hz, 1H), 6.02 (d, $J = 1.3$ Hz, 1H), 5.93 (d, $J = 1.3$ Hz, 1H), 5.44 (d, $J = 4.1$ Hz, 1H), 4.46 (d, $J = 4.3$ Hz, 1H), 4.14 (s, 3H), 4.10 (s, 3H), 3.89 (s, 3H), 2.65–2.51 (m, 4H), 2.20–2.00 (m, 2H), 1.70–1.56 (m, 1H); ^{13}C NMR ($CDCl_3$, 75 MHz): δ 167.9, 152.4, 147.5, 146.0, 140.5, 140.0, 134.9, 133.2, 128.7, 126.7, 126.6, 124.1, 120.5, 118.1, 117.2, 114.7, 100.9, 81.8, 62.2, 61.0, 59.5, 56.5, 50.7, 46.7, 29.6, 27.2; IR (KBr): 3,413, 2,948, 1,765, 1,614, 1,497, 1,422, 1,237, 1,158, 1,120, 1,039, 946, 806, 732, 701 cm^{-1}; MS (ESI): m/z 580 $(M + Na)^+$; HRMS (ESI): Calcd. for $C_{29}H_{26}NO_7F_3Na$ $(M + Na)^+$, 580.1559; found: 580.1568.

*Ethyl 2-chloro-5-((R)-5-((S)-4,5-dimethoxy-3-oxo-1,3-dihydroisobenzofuran-1-yl)-4-methoxy-6-methyl-5,6,7,8-tetrahydro-[1,3]dioxolo [4,5-g]isoquinolin-9-yl)benzoate (**5b**)* Yield: 70 %; m.p: 152 °C; $[\alpha]_D^{25} = -127.28$ ($c = 1$, dichloromethane); ^1H NMR ($CDCl_3$, 300 MHz): δ 7.64 (d, $J = 2.0$ Hz, 1H), 7.45 (d, $J = 8.3$ Hz, 1H), 7.34–7.27 (dd, $J = 2.0, 8.1$ Hz, 1H), 7.26 (s, 1H), 7.02 (d, $J = 8.1$ Hz, 1H), 6.16–6.05 (d, $J = 7.9$ Hz, 1H), 6.00 (s, 1H), 5.92 (s, 1H), 5.45 (d, $J = 3.7$ Hz, 1H), 4.49–4.34 (m, 3H), 4.10 (s, 6H), 3.91 (s, 3H), 2.72–2.53 (m, 4H), 2.26–2.09 (m, 2H), 1.66 (s, 1H), 1.42 (t, $J = 7.1$ Hz, 3H); ^{13}C NMR ($CDCl_3$, 75 MHz): 167.9, 165.6, 152.3, 147.6, 146.0, 140.8, 140.1, 133.8 133.7, 132.9, 132.5, 130.8, 130.5, 130.3, 120.4, 118.1, 117.7, 117.6, 114.1, 100.9, 81.8, 62.9, 61.6, 61.0, 59.5, 56.8, 50.5, 46.6, 26.9, 14.1; IR (KBr): 3,418, 2,922, 2,853, 2,795, 1,756, 1,633, 1,597, 1,498, 1,363, 1,274, 1,159, 1,036, 940, 813, 728, 506 cm^{-1}; MS (ESI): *m/z* 618 $(M + Na)^+$; HRMS (ESI): *m/z* Calcd. for $C_{31}H_{30}NO_9ClNa$ $(M + Na)^+$, 618.1506; found: 618.1476.

*Ethyl 4-((R)-5-((S)-4,5-dimethoxy-3-oxo-1,3-dihydroisobenzofuran-1-yl)-4-methoxy-6-methyl-5,6,7,8-tetrahydro-[1,3]dioxolo[4,5-g]isoquinolin-9-yl)benzoate (**5c**)* Yield: 67 %; m.p: 143 °C; $[\alpha]_D^{25}$: −140.52 ($c = 1$, dichloromethane); ^1H NMR ($CDCl_3$, 300 MHz): δ 8.09 (d, $J = 8.4$ Hz, 2H), 7.33 (d, $J = 8.3$ Hz, 2H), 7.03 (d, $J = 8.3$ Hz, 1H), 6.16 (d, $J = 8.1$ Hz, 1H), 6.00 (d, $J = 1.3$ Hz, 1H), 5.93 (d, $J = 1.3$ Hz, 1H), 5.54 (d, $J = 4.1$ Hz, 1H), 4.49 (d, $J = 4.3$ Hz, 1H), 4.40 (q, $J = 7.1$ Hz, 2H), 4.12 (s, 3H), 4.11 (s, 3H), 3.91 (s, 3H), 2.67–2.52 (m, 4H), 2.27–2.11 (m, 2H), 1.76–1.65 (m, 1H), 1.41 (t, $J = 7.1$ Hz, 3H); ^{13}C NMR ($CDCl_3$, 75 MHz): δ 167.9, 166.2, 152.3, 147.7, 146.0, 140.9, 140.0, 138.9, 133.7, 130.6, 130.0, 129.3, 120.5, 118.1, 117.7, 117.7, 115.4, 100.9, 81.8, 62.2, 61.1, 60.9, 59.5, 56.9, 56.7, 46.7, 27.0, 14.3; IR (KBr): 3,413, 2,915, 1,767, 1,697, 1,616, 1,498, 1,464, 1,443, 1,381, 1,306, 1,262, 1,165, 1,088, 1,034, 1,012, 821, 621 cm^{-1}; MS (ESI): m/z 584 $(M + Na)^+$; HRMS (ESI): *m/z* Calcd. for $C_{31}H_{31}NO_9Na$ $(M + Na)^+$, 584.1896; found: 584.1881.

*(S)-6,7-Dimethoxy-3-((R)-4-methoxy-6-methyl-9-(4-vinylphenyl)-5,6,7,8-tetrahydro-[1,3]dioxolo [4,5-g]isoquinolin-5-yl)isobenzofuran-1(3H)-one (**5d**)* Yield: 60 %; m.p: 120 °C; $[\alpha]_D^{25} = -120.22$ ($c = 1$, dichloromethane); ^1H NMR ($CDCl_3$, 300 MHz): δ 7.40 (d, $J = 8.2$ Hz, 2H), 7.17 (d, $J = 8.0$ Hz, 2H), 6.97 (d, $J = 8.1$ Hz, 1H),

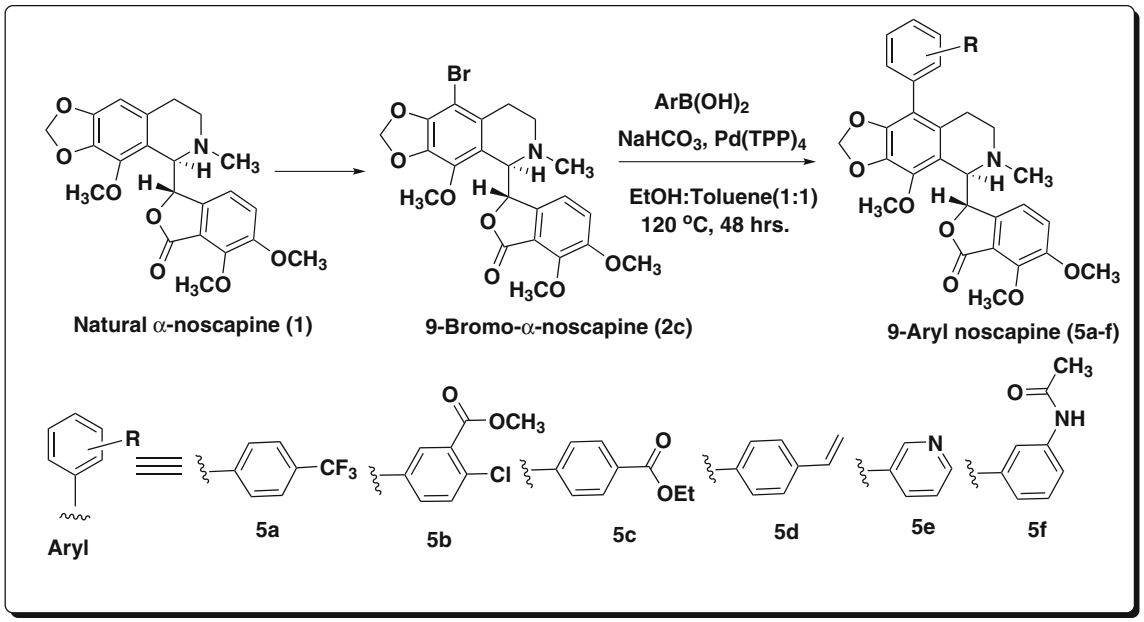

Fig. 4 Optimized Suzuki coupling reaction conditions for the synthesis of noscapine derivatives **5a**–**5f**

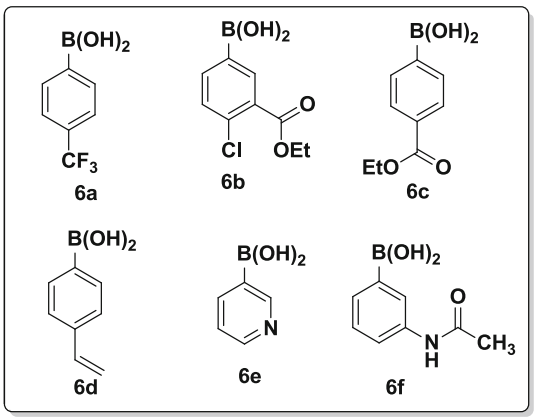

Fig. 5 Aryl boronic acids **6a**–**6f** used in the present study

6.74–6.66 (dd, $J = 10.8$ Hz, 17.5 Hz, 1H) 6.10 (s, 1H), 5.98 (s, 1H), 5.91 (s, 1H), 5.74 (d, $J = 17.5$ Hz, 1H), 5.48 (s, 1H), 5.25 (d, $J = 10.8$ Hz, 1H), 4.47 (s, 1H), 4.10 (s, 6H), 3.90 (s, 3H), 2.66–2.54 (m, 4H), 2.27–2.13 (m, 2H), 1.77–1.64 (m, 1H);^{13}C NMR (75 MHz, $CDCl_3$): δ 157.9, 152.2, 147.7, 146.0, 143.6, 140.9, 139.6, 136.7, 133.7, 133.5, 130.7, 130.1, 126.0, 120.4, 117.8, 116.1, 114.2, 100.8, 81.9, 62.3, 61.1, 59.5, 56.9, 50.8, 46.6, 27.0, 23.2, 29.6; MS (ESI): *m/z* 538$(M + Na)^+$; HRMS (ESI): Calcd. for $C_{30}H_{29}NO_7Na$ $(M + Na)^+$, 538.1841; found: 538.1848.

*(S)-6,7-Dimethoxy-3-((R)-4-methoxy-6-methyl-9-(pyridin-3-yl)-5,6,7,8-tetrahydro-[1,3]dioxolo[4,5-g]isoquinolin-5-yl) isobenzofuran-1(3H)-one (**5e**)* Yield: 62 %; m.p: 193 °C; $[\alpha]_D^{25}$: −124.25 ($c = 1$, dichloro methane); ^{1}H NMR ($CDCl_3$, 500 MHz): δ8.52 (s, 1H), 8.43 (s, 1H) 7.56 (d, $J = 7.6$ Hz, 1H), 7.30 (t, $J = 6.6$ Hz, 1H), 6.98 (d, $J = 8.5$ Hz, 1H), 6.12 (d, $J = 7.6$ Hz, 1H), 5.99 (s, 1H), 5.92 (s, 1H), 5.43 (d, $J = 4.7$ Hz, 1H), 4.43 (d, $J = 4.7$ Hz, 1H), 4.11 (s, 3H), 4.08 (s, 3H), 3.88 (s, 3H), 2.67–2.60 (m, 1H), 2.55 (s, 3H), 2.22–2.14 (m, 2H), 1.79–1.69 (m, 1H); ^{13}C NMR ($CDCl_3$, 75 MHz): 167.9, 152.3, 150.7,148.36, 147.6, 146.4, 140.7, 140.2, 137.3, 133.7, 130.7, 130.3, 130.2, 123.1, 120.4, 118.2, 117.5, 100.9, 81.8, 62.2, 61.0, 59.4, 56.8, 50.6, 46.6, 26.8; IR (KBr): 3,412, 2,938, 1,756, 1,637, 1,497, 1,445, 1,273, 1,082, 1,032, 943, 815, 714, cm^{-1}; MS (ESI): m/z 513 $(M + Na)^+$; HRMS (ESI): Calcd. for $C_{27}H_{26}N_2O_7Na$ $(M + Na)^+$, 513.1637; found: 513.1615.

*N-(3-((R)-5-((S)-4,5-Dimethoxy-3-oxo-1,3-dihydroisobenzofuran-1-yl)-4-methoxy-6-methyl-5,6,7,8-tetrahydro-[1,3]-dioxolo[4,5-g]isoquinolin-9-yl)phenyl)acetamide (**5f**)* Yield: 55 %; m.p: 240 °C; $[\alpha]_D^{25} = -138.68$ ($c = 1$, dichloromethane); ^{1}H NMR ($CDCl_3$, 300 MHz) δ 7.68 (s, 1H), 7.46–7.28 (m, 2H), 7.25–7.12 (d, $J = 8.3$ Hz, 1H), 7.07–6.93 (d, $J = 7$ 0.17 Hz, 1H), 6.23–6.10 (d, $J = 8.3$ Hz, 1H), 5.98 (s, 1H), 5.91 (s, 1H), 5.54 (d, $J = 3.9$ Hz, 1H), 4.50 (d, $J = 3.9$ Hz, 1H), 4.10 (s, 6H), 3.94 (s, 3H), 2.54 (s, 4H), 2.27–2.10 (m, 5H), 1.77–1.60 (m, 1H); ^{13}C NMR ($CDCl_3$, 75 MHz): δ 168.4, 152.2, 147.3, 145.9, 140.6, 139.5, 138.2, 134.9, 133.6, 130.8, 128.5, 125.5, 121.3, 120.2, 118.3, 117.9, 117.6, 116.3, 100.8, 82.1, 62.1, 61.0, 59.4, 56.6, 56.4, 50.8, 46.7, 27.0, 24.4; IR (KBr): 3,329, 2,920, 2,791, 1,739, 1,682, 1,586, 1,548, 1,503, 1,384, 1,274, 1,086, 1,037,797, 620 cm^{-1}; MS (ESI): m/z 569 $(M + Na)^+$; HRMS (ESI):

Calcd. for $C_{30}H_{30}N_2O_8Na$ $(M + Na)^+$, 569.1899; found: 569.1920.

X-ray crystallography

X-ray data for the compound **5b** was collected at room temperature using a Bruker Smart Apex CCD diffractometer with graphite monochromated MoKα radiation (λ = 0.71073 Å) with ω-scan method [45]. Preliminary lattice parameters and orientation matrices were obtained from four sets of frames. Integration and scaling of intensity data was accomplished using SAINT program [46]. The structure was solved by direct methods using SHELXS97 [46] and refinement was carried out by full-matrix least-square technique using SHELXL97 [46]. Anisotropic displacement parameters were included for all non-hydrogen atoms. All H atoms were located in different Fourier maps and subsequently geometrically optimized and allowed as riding atoms, with C–H = 0.93–0.97 Å, with $U_{iso}(H) = 1.5U_{eq}(C)$ for methyl H or $1.2U_{eq}(C, N)$. The methyl groups were allowed to rotate but not to tip. The absolute configuration of the procured material was known in advance and was confirmed by unambiguous refinement of the absolute structure parameter [47] for **5b**.

Crystal structure data for **5b**: $C_{31}H_{30}ClNO_9$, $M = 596.01$, colorless block, $0.21 \times 0.18 \times 0.12$ mm^3, monoclinic, space group $P2_1$ (No. 4), $a = 12.9325(12)$, $b = 8.2237(7)$, $c = 13.3317(12)$ Å, $\beta = 92.1170(10)°$, $V = 1416.9(2)$ Å^3, $Z = 2$, $D_c = 1.397$ g/cm^3, $F_{000} = 624$, CCD Area Detector, MoKα radiation, $\lambda = 0.71073$ Å, $T = 294(2)$K, $2\theta_{max} = 50.0°$, 13,429 reflections collected, 4,953 unique ($R_{int} = 0.0232$). Final *GooF* = 1.107, *R1* = 0.0461, *wR2* = 0.1294, *R* indices based on 4,644 reflections with $I > 2\sigma(I)$ (refinement on F^2), 384 parameters, one restraint, $\mu = 0.193$ mm^{-1}. Absolute structure parameter = 0.12(10) [46]. CCDC 944747 contains supplementary Crystallographic data for the structure. These data file can be obtained free of charge at www.ccdc.cam.ac.uk/conts/retrieving.html [or from the Cambridge Crystallographic Data Centre (CCDC), 12 Union Road, Cambridge CB2 1EZ, UK; fax: +44(0) 1223 336 033; email: deposit@ccdc.cam.ac.uk].

Biology

Cell lines and chemicals

Cell culture reagents were obtained from Sigma (location) and Invitrogen (location). MCF-7, a human breast epithelial cancer cell line; HeLa, a human cervix cell line and A549, a human lung cancer cell line were obtained from the National Repository of Animal Cell Culture, National Centre for Cell Sciences, Pune (NCCS), India. The cell lines were maintained in Dulbecco's Modification of Eagle's Medium 1X (DMEM) with 4.5 g/L glucose and L-glutamine (Sigma) supplemented with 10 % fetal bovine serum (Invitrogen) and 1 % penicillin/streptomycin (Invitrogen).

In vitro cell proliferation assays (MTS assay)

A panel of three human cancer cell lines (MCF-7, HeLa and A549) were seeded into 96-well plates at a density of 5×10^3 cells per well and were treated with increasing gradient concentrations of noscapinoids **5a–5f** for 72 h. Measurement of cell proliferation was performed colorimetrically by 3-(4,5-dimethylthiazol-2-yl)-5-(3-carboxymethoxyphenyl)-2-(4-sulphophenyl)-2H-tetrazolium, inner salt (MTS) assay, using the CellTiter96 aqueous one solution reagent (Sigma). Cells were exposed to MTS for 3 h and absorbance was measured using a microplate reader (Molecular Devices, Sunnyvale, CA, USA) at an optical density (OD) of 490 nm. The percentage of cell survival as a function of drug concentration was then plotted to determine the IC_{50} value, which stands for the drug concentration needed to prevent cell proliferation by 50 %.

Tubulin purification

Tubulin was purified from bovine brain by cycles of temperature-dependent assembly and disassembly as described previously [48, 49]. The concentration of the tubulin was determined by the method of Bradford using BSA as the standard [50]. Purified tubulin was quickly frozen and stored at −80 °C until used.

Tubulin binding assay

A fluorescence titration probing the quenching patterns of intrinsic tryptophan fluorescence of tubulin in the presence of different concentrations of the compounds (**5a–5f)** was used for determining the tubulin binding affinity of noscapinoids [20]. In brief, the compounds (concentration range 0–200 μM) were incubated with 2 μM tubulin in PEM buffer (100 mM PIPES, pH 6.8, 3mM $MgSO_4$, and 1 mM EGTA) for 45 min at 37 °C. The relative intrinsic fluorescence intensity of tubulin was then monitored in a Varian Cary Eclipse fluorescence spectrophotometer (Agilent Technologies, CA, USA) using a quarts cuvette of 0.3 cm path length. The samples were excited at 295 nm and the emission peaks at 335 nm were recorded. The fluorescence emission intensity of noscapinoids at this excitation wavelength was negligible. The use of a 0.3 cm path-length cuvette minimized the inner filter effects caused by the absorbance of the compound. In addition, the inner filter effects were corrected using a formula

Table 1 Grouping of the experimental animals and the doses and duration of treatment

Groups	No. of animals	Sex	Dose/day	Duration of dose (days)	Frequency
(1) Vehicle treated (control)	5	Male	0.1 % DMSO	28	Daily
(2) Vehicle treated (control)	5	Female	0.1 % DMSO	28	Daily
(3) Drug treated	5	Male	300 mg/kg	28	Daily
(4) Drug treated	5	Female	300 mg/kg	28	Daily
(5) Drug treated	5	Male	600 mg/kg	01	Once
(6) Drug treated	5	Female	600 mg/kg	01	Once

$F_{corrected} = F_{observed}$·antilog $[(A_{ex} + A_{em})/2]$, where A_{ex} is the absorbance at the excitation wavelength and A_{em} is the absorbance at the emission wavelength. The dissociation constant (K_d) was determined by the formula: $1/\boldsymbol{a} = K_d/[\text{free ligand}] + 1$, where $\boldsymbol{a}$ is the fractional occupancy and [free ligand] is the concentration of the free noscapinoid molecule. Two independent experiments were performed for each compound.

Cell cycle analysis

The flow cytometric evaluation of the cell cycle progression in the presence of the noscapinoids was performed as described previously [51]. Briefly, cancer cells (MCF-7) were incubated with 25 μM concentration of the noscapinoids, **5a**–**5f**. Cells were sampled at three time periods 24, 48 and 72 h and analysed using flow cytometry. After the incubation, 2×10^6 cells were centrifuged, washed twice with cold phosphate buffered saline (PBS) and fixed in 70 % ethanol. Tubes containing the cell pellets were stored at 4 °C for at least 24 h. The pellets were resuspended in 30 μl of phosphate/citrate buffer (0.2 M Na_2HPO_4/0.1 M citric acid, pH 7.5) at room temperature for 30 min and centrifuged at 1,000×*g* for 10 min and the supernatant was discarded. The pellets were washed twice with 5 ml PBS and stained with propidium iodide (0.5 ml; 0.1 in 0.6 % Triton-X in PBS) and 0.5 ml of RNase A (2 mg/mL) for 45 min in the dark. Samples were then analyzed on a FACS Calibur flow cytometer (Beckman Coulter Inc., Fullerton, CA, USA).

Toxicological evaluation of the noscapinoids

The noscapinoid, **5e,** which showed better anti-proliferative activity against cancer cells and K_d value against tubulin among the newly designed analogues was used for toxicological analysis in animals. Swiss albino mice used for the toxicological study were bred and maintained in the Animal Facility of School of Pharmacy, Guru Ghasidas Central University, Bilaspur, Chhattisgarh, India. All experimental protocols involved in this study were approved by Institutional Animal Ethics Committee (Ref. No.: 994/a/GO/06/CPCSEA) and were reviewed by the committee for the purpose of control and supervision of experiments on animals. 3 months old male and female Swiss albino mice, with an average weight of 25 g were used for the experiments. Water and food pellets (Lipton Pvt. Ltd., India) were given ad libitum. Animals were maintained in the animal house at 12 h light: 12 h dark cycle (Light 7:00 a.m.–7:00 p.m.). Temperature and humidity were maintained at 24–28 °C and 55–60 %, respectively.

Drug treatment (preparation of drug and pharmacological administration)

Swiss albino mice (n = 30) were randomly divided into six experimental groups of five animals each for the study (Table 1). The animals in group 1 and 2 served as control for male and female mice respectively. The animals in group 3 and 4 were administered oral doses of 300 mg/kg body weight daily up to 28 days. Similarly, the animals in group 5 and 6 were administered once a single dose of 600 mg/kg body weight (Table 1). The above dose of 300 mg/kg was chosen on the basis of previous study [51] and the dose of 600 mg/kg was selected on the basis of reported LD_{50} dose (602 ± 31 mg/kg) [52] of noscapine for mice. The compound was dissolved in 0.1 % DMSO in distilled water and administered orally using a feeding cannula. The animals were continuously monitored for food and water intake and body weights on a daily basis. Both the doses were well tolerated and the mice did not show any signs of discomfort.

Histology and hematology

At the end of the experiment, animals in group 1–4 were sacrificed on day 28, whereas animals in group 5 and 6 were sacrificed on day 14. Blood was collected from the normal or treated mice on the day of sacrifice directly from the heart in heparinized tubes and analyzed on a complete blood count instrument (CDC Technologies, Oxford, CT, USA). For histological studies, mice of different groups

were anesthetized with sodium pentobarbital and were perfused with 4 % paraformaldehyde in PBS (pH 7.4). The vital organs such as brain, duodenum, liver, lungs, kidney, heart and spleen were removed, post fixed in 4 % paraformaldehyde in PBS and further processed for histopathological analysis. Tissues were embedded in paraffin, sectioned using a microtome and 5 μm sections were stained with hematoxylin and eosin. The stained sections were analyzed for microscopic evaluation at magnification 200× and 400× using bright field microscope (Olympus, CX31, Japan).

Results and discussion

The effectiveness in terms of cell killing of the lead compound, noscapine was improved manyfold by synthesizing many potent derivatives. These derivatives were proven to have increased tubulin binding affinity as indicated by their lower dissociation constants (K_d) from 152 μM for noscapine to 86 μM for nitro noscapine, 80 μM for F-noscapine, 54 μM for Br-noscapine, 40 μM for Cl-noscapine, 22 μM for I-noscapine and 14 μM for amino-noscapine [19, 43, 44]. Furthermore, recently we have made some effective derivatives of noscapine by functionalization of 'N' in isoquinoline unit of natural α-noscapine [21]. Availability of structure activity data of these derivatives of noscapine led us to develop a reasonable predictive model for predicting the binding affinity of newly designed derivatives and screening. In continuation of our efforts to develop new derivatives of noscapine, we are reporting in this study a series of biaryl pharmacophore inserted noscapine derivatives **5a**–**5f** as potent anticancer agents.

Molecular modelling study

Binding mode and binding affinity of designed noscapinoids

The molecular interaction and binding affinities of designed noscapinods, **5a**–**5f** onto tubulin were calculated, applying molecular docking in combination with MM-PBSA and MM-GBSA calculations. The initial structure of tubulin was obtained from the PDB database. The gaps were filled based on homology model building and further refined using MD simulation. The relative fluctuation in the root-mean-square deviations (RMSDs) of the Cα atoms of tubulin (αβ heterodimmer) is very small after the initial equilibration (∼4 ns), demonstrating the convergence of the simulation (Fig. 6). Noscapinoids, newly designed in this study (Fig. 2) and the previously reported (Fig. 3) were docked into the reported binding site of noscapinoids [31] using Glide XP (extra precision) and evaluated using a Glide XP_{score} function [32, 33]. The newly designed noscapinoids **5a**–**5f** showed better docking scores ranging from −8.466 to −6.085 kcal/mol than the parent compound, noscapine (−5.505 kcal/mol) (Table 2). Some of the derivatives even showed better docking score in comparison to the previously reported noscapinoids.

To estimate the free energy change that describes the binding of newly designed noscapinoids **5a**–**5f** with tubulin, we calculated the difference between the free energy of the complex and that of the respective binding partners based on MM-PBSA and MM-GBSA methods. Energy values were calculated as the average value out of 1,000 snapshots generated from the last 2 ns of the MD trajectory for each tubulin–noscapinoid complex. The convergence of the MD trajectories was monitored by plotting RMSD of the backbone C_α atoms with respect to time. In fact, the relative fluctuation of the RMSD value is very small after ∼8 ns suggesting the stability of the system (Fig. 6). Furthermore, the root mean square fluctuations (RMSF) of the residues of tubulin involved in the interaction with the ligands (within 20 Å diameters) in the bound form and in the free form were calculated to reveal the flexibility of these residues (Fig. 7). In fact, the RMSF values of these residues in the bound form were slightly lower compared to free form, indicating that these residues seem to be more rigid as a result of binding to noscapinoids. Different levels of flexibility of these residues have also been noticed in the bound form of tubulin across various ligands (Fig. 7). This may be because of subtle differences in the mode of molecular interactions of noscapinoids that perhaps

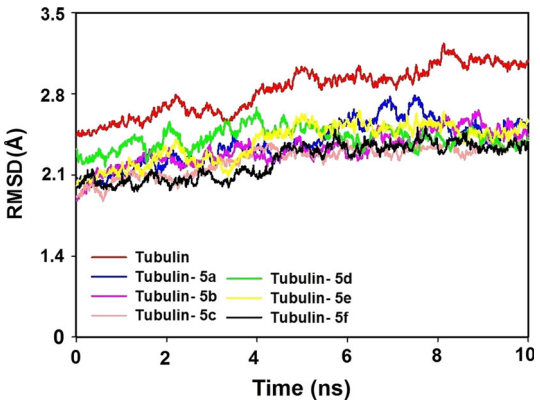

Fig. 6 The root-mean square deviations (RMSD) of Cα carbon atoms of tubulin during 10 ns of MD simulation of tubulin–ligand complexes with respect to initial structure as a function of time. The relative fluctuation in the RMSD of the Cα atoms is very small after ∼8 ns of the simulation, demonstrating the convergence of the simulation. A 10 ns MD simulation was carried out with a time step of 2 fs, a total of 5,000 frames were generated and the last 1,000 frames from each molecular species were used to generate the average structure

Table 2 Molecular docking results (Glide XP) as well as calculated energies based on LIE–SGB model of newly designed noscapinoids (**5a–5f**): van der Waals (vdw), electrostatic (elec), cavity (cav), predicted and experimental binding free energy (ΔG_{bind})

Ligand	Glide XP_{score} (kcal/mol)	$\langle U_{vdw} \rangle$ (kcal/mol)	$\langle U_{elec} \rangle$ (kcal/mol)	$\langle U_{cav} \rangle$ (kcal/mol)	Predicted ΔG_{bind} (kcal/mol)	K_d value (μM)	Experimental ΔG_{bind} (kcal/mol)
5a	−6.085	−60.57	41.82	1.05	−5.568	126 ± 5.0	−5.325
5b	−6.397	−60.68	50.47	1.62	−5.954	–	–
5c	−6.833	−59.44	53.78	1.23	−5.689	107 ± 5.0	−5.422
5d	−6.845	−63.89	63.01	0.49	−5.732	71 ± 4.0	−5.665
5e	−7.717	−63.21	61.54	1.07	−5.965	68 ± 6.0	−5.691
5f	−7.466	−67.39	44.45	0.78	−5.961	–	–

Experimental ΔG_{bind} was calculated from the dissociation constant (K_d value) using the relationship: $\Delta G_{bind} = RT \ln K_d$ where T = 298 K and R = 0.00199 (kcal/mol K). Predicted ΔG_{bind} was calculated using LIE–SGB empirical equation: $\Delta G_{bind} = 0.0762\langle U_{vdw} \rangle - 0.00965\langle U_{elec} \rangle - 0.520\langle U_{cav} \rangle$

account for their net effect on the binding free energy change with tubulin. All the noscapinoids (**5a–5f)** are well accommodated into the binding site, at the interface between α- and β-tubulin (Fig. 8). However, their binding modes inside the binding cavity are distinct as shown in Fig. 9. The binding mode was represented in two steps: (a) receptor residues that have strong interactions with the ligand such as a favorable hydrogen-bonding interaction and (b) receptor residues that are close to the ligand, but whose interactions with the ligand are weak or diffuse, such as hydrophobic interaction. The differences in binding modes of these noscapinoids **5a–5f** are not only due to various substitutions of functional groups in the scaffold structure but also because of differential contribution in binding free energy of amino acids involved in the interactions. Binding free energy of individual amino acid involved in the interaction with these ligands was calculated based on MM-GBSA and plotted in Fig. 10. Around 9–11 residues contribute considerable binding energy with noscapinoids **5a–5f**, each yielding <−1.0 kcal/mol of free energy (Fig. 10a–f). The analysis reveals that Leu 253 is a consistently important contributor to the binding energy among all the noscapinoids.

Furthermore, to determine the detailed contribution of each important residue, the binding energy was decomposed into several other components (the electrostatic, van der Waals, and solvation) and plotted in Fig. 11. As an example, in the tubulin-**5a** complex, Lys 252 has an appreciable solvation energy (δE_{sol}) contribution, with a δE_{sol} of ≤−7 kcal/mol, while electrostatic interaction (δE_{ele}) shows unfavorable contributions at >6 kcal/mol, as a result the total energy contributions of Lys 252 is weak (Fig. 11a). For tubulin-**5b** complex, the residue Asp 249 has large electrostatic contribution ($\delta E_{ele} \leq -4$ kcal/mol), while the residue Lys 252 has large solvation contribution ($\delta E_{sol} \leq -7$ kcal/mol). Apropos to this Asp 249 has an unfavorable solvation contribution ($\delta E_{sol} \geq 15$ kcal/mol) and Lys 252 has an unfavorable electrostatic contribution ($\delta E_{ele} \geq 7$ kcal/mol) to the complex, resulting in weak contributions to the total energy for both the residues. Similarly, for tubulin-**5c** complex, the electrostatic interactions of Thr 178 and Asn 256 are −6.5 and −3.0 kcal/mol, respectively, which suggests that both are key residues in the binding of **5c**. In the tubulin-**5d** complex, Lys 252 has the strongest solvation energy contribution ($\delta E_{sol} \leq -4$ kcal/mol), while the residues Lys 252 and Lys 350 contributed maximum of solvation energy ($\delta E_{sol} \leq -7$ and ≤−4 kcal/mol respectively) towards the binding of **5f** with tubulin.

The calculated binding energy ($\Delta G_{bind,\ PB(GB)}$) of the noscapinoids **5a–5f** with tubulin calculated according to MM-PBSA and MM-GBSA is summarized in Table 3. The calculated binding energy based on both the methods indicate strong interactions of newly designed noscapinoids with tubulin in the following order of magnitude: **5e** > **5f** > **5d** > **5c** > **5b** > **5a**. The derivative **5e** showed the highest binding energy of −48.27 and −42.34 kcal/mol using both MM-PBSA and MM-GBSA methods. Both the intermolecular van der Waals (ΔE_{vdw}) and the electrostatic (ΔE_{ele}) interactions are significant contributors to the binding, whereas the polar solvation terms ($\Delta G_{PB(GB)}$) counteract binding. In contrast, non-polar solvation terms ($\Delta G_{sol\text{-}np}$), which correspond to the burial of solvent-accessible surface-area upon binding, contribute slightly favorably. Though the gas-phase electrostatic value (ΔE_{gas}) is in favor of the binding of all the noscapinoids, the overall electrostatic interaction energy ($\Delta G_{ele,\ PB(GB)}$) is positive and unfavorable for the binding, perhaps due to large desolvation penalty of charged and polar groups that are not sufficiently compensated by complex formation. Comparing the net polar ($\Delta G_{PB(GB)} + \Delta E_{ele}$) and nonpolar energies ($\Delta G_{sol\text{-}nonpolar} + \Delta E_{vdw}$) contributions, we noticed that the binding of noscapinoids onto tubulin is mainly driven by nonpolar interaction.

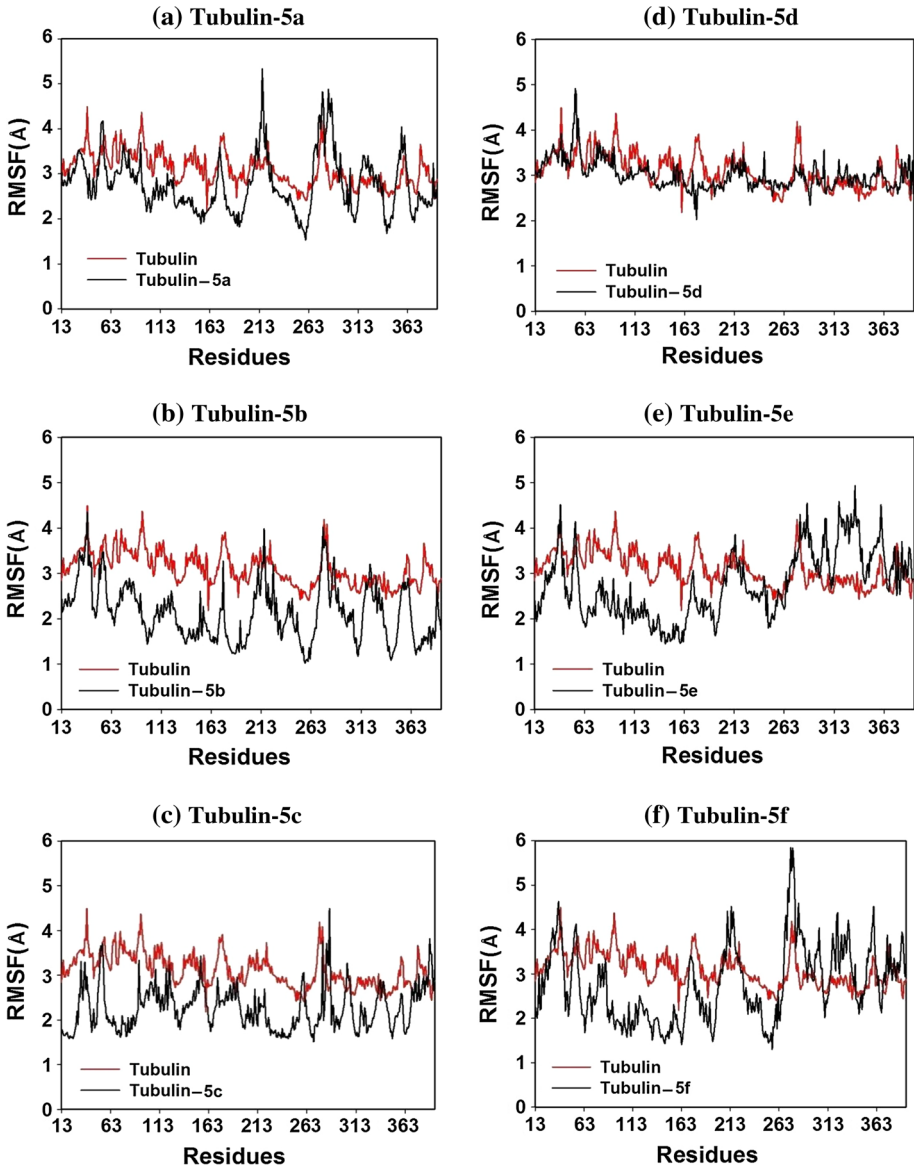

Fig. 7 Root mean square fluctuation (RMSF) of the residues of tubulin within 20 Å diameter (includes 13–393 residues) of the docked ligands in the bound form and in the unbound form of tubulin heterodimer. Different levels of flexibility of these residues were noticed in the bound form of tubulin with different noscapinoids. Most of the residues in the binding site showed flexibilities <5 Å in case of tubulin bound to noscapinoids as compared to the free tubulin heterodimer, indicating that these residues seem to be more rigid as a result of binding

*Predictive binding affinity of **5a–5f** with tubulin (LIE–SGB calculation)*

The binding affinity ($\Delta G_{bind,\ pred}$) of newly designed noscapinoids with tubulin was predicted based on computationally developed LIE, utilizing the experimental activity of training set molecules. Since the molecular docking predicts accurate binding pose for the ligands onto the receptor, we have used the docking complexes of noscapinoids with tubulin and performed hybrid Monte Carlo simulation with generalized Born (SGB) continum solvation model to develop a robust predictive model. Towards this end we have used the experimental binding energy of previously reported 12 noscapinoids as training set. The various interaction energy terms used in the model were included in Table 4 and are used to develop the LIE model. The values obtained for the three fitting parameters, α, β and γ are 0.076, −0.010 and −0.520, respectively. The largest contribution for the binding free energy comes from the van der Waals interactions. The predicted ΔG_{bind} of the training set molecules based on LIE model is very close to the experimental ΔG_{bind} (root mean square error was 0.288 kcal/mol). The quality of the fit can also be judged by the value of the squared correlation coefficient (R^2) and analysis of variance (F-value).

$$\Delta G_{bind,pred} = 0.076\langle U_{vdw}\rangle - 0.010\langle U_{elec}\rangle - 0.520\langle U_{cav}\rangle \quad (2)$$

$$(n = 12,\ R^2 = 0.776,\ s = 0.26,\ F = 1969.8,\ P = 0.001,\ PRESS = 1.243)$$

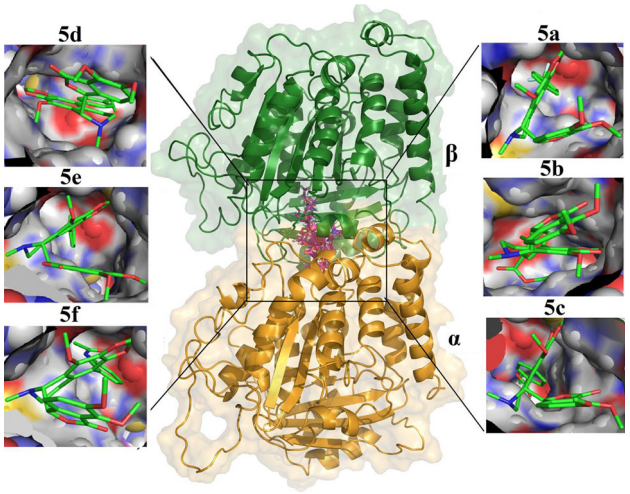

Fig. 8 The newly designed noscapinoids **5a**–**5f** are well accommodated in the noscapinoid binding site at the interface between α- and β-tubulin. Snapshot of the ligands **5a**–**5f** are obtained from the MD simulation. The binding site is represented as macromodel surface according to residue charge (electropositive charge, *blue*; neutral, *yellow* and electronegative charge, *red*) as implemented in Pymol

Because of high predictability, the LIE model was used to predict the ΔG_{bind} of the newly designed noscapinoids. All the derivatives revealed improved predicted binding energy (ranging from −5.568 to −5.965 kcal/mol) in comparison to the lead molecule (−5.214 kcal/mol). The derivative **5e** showed highest binding affinity ($\Delta G_{bind,pred}$) of −5.965 kcal/mol in the series. Inspired by our computational findings, we have made an attempt to synthesize the newly designed noscapinoids to further evaluate their experimental activities.

Chemical synthesis of **5a**–**5f**

Synthesizing the derivatives of noscapine is always challenging because of its highly sensitive C–C bond between isoquinoline and isobenzofuranone ring components which is labile to strong acids and base. However, we have optimized the reaction conditions for the synthesis of these derivatives **5a**–**5f** from 9-bromonoscapine **2c** as starting material without affecting the sensitive C–C bond. The

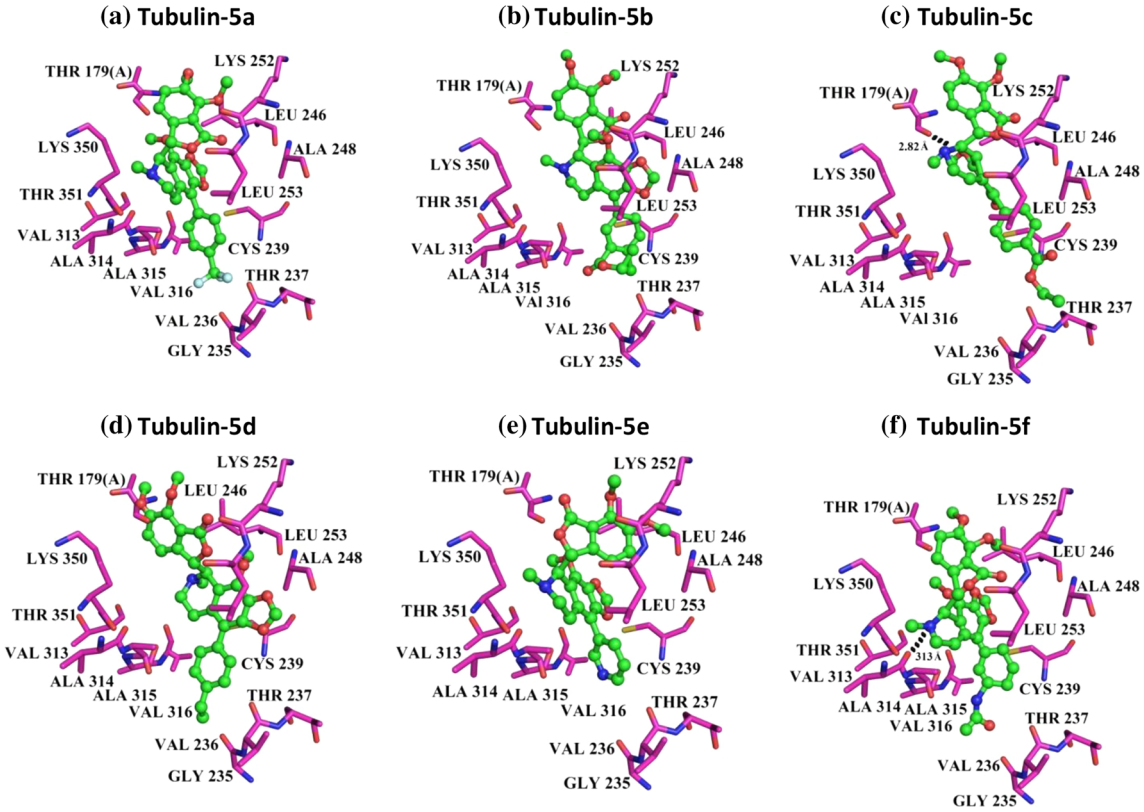

Fig. 9 Typical snapshot of the binding mode of noscapinoids **5a**–**5f** within the noscapinoid binding site [30] of tubulin. The hydrogen bonds formed (if any) are represented as *dotted lines*. The noscapinoid **5c** forms one hydrogen bond with Thr 179 of the α chain. The nitrogen atom N1 of the upper isoquinalone ring hydrogen bonds with oxygen atom of Thr 179 with a distance of 2.82 Å. The noscapinoid **5f** forms one hydrogen bond with Val 313 of the β chain. The nitrogen atom N1 of the upper isoquinalone ring hydrogen bonds with oxygen atom of Val 313 with a distance of 3.13 Å. The other noscapinoids however do not involve any hydrogen bonds. The difference in binding modes of these noscapinoids is due to various substitutions in the scaffold structure. The amino acids Thr 366 and Ile 368 are not shown for better clarity

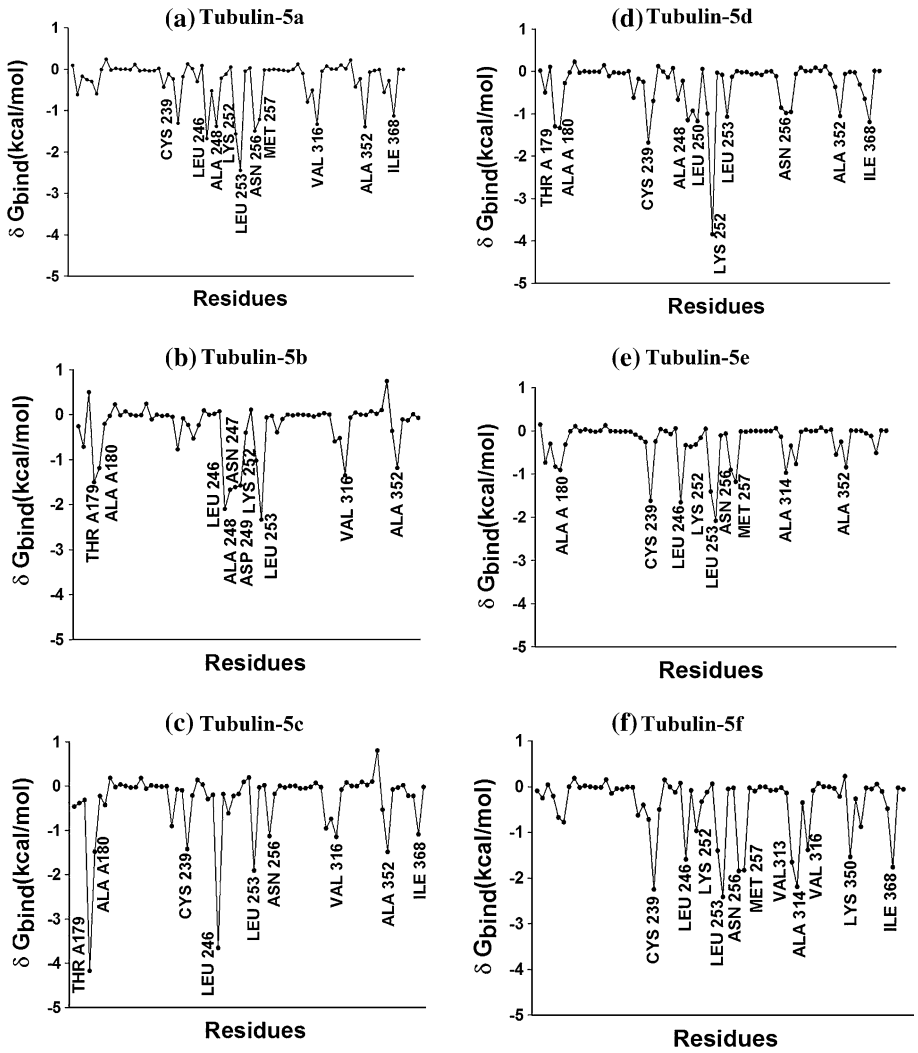

Fig. 10 Total binding energy (δG_{bind}) contribution of amino acids within and around binding site (12 Å of the docked ligand) of tubulin involved in interaction with noscapinoids **5a–5f**. Around 9–11 residues contribute considerable binding energy with noscapinoids **5a–5f** respectively, each yielding <−1.0 kcal/mol of free energy. However, Leu 253 is a consistently important contributor to the binding energy

Table 3 Calculated binding energy and its components (kcal/mol) of noscapine derivatives (**5a–5f**) binding with tubulin

Energy components (kcal/mol)	5a	5b	5c	5d	5e	5f
ΔE_{ele}	−320.1	−318.6	−318.2	−314.7	−42.95	−340.7
ΔE_{vdw}	−66.03	−69.19	−74.87	−68.41	−51.42	−72.01
ΔE_{gas}	−386.2	−387.8	−393.0	−383.1	−94.36	−412.7
$\Delta G_{sol\text{-}np}$	−7.593	−7.906	−8.629	−7.070	−5.953	−7.857
ΔG_{PB}	356.2	357.7	362.6	345.8	56.82	375.5
$\Delta G_{solv,\ PB}$	351.1	351.8	356.5	340.9	52.02	370.3
$\Delta G_{ele,\ PB}$	36.08	39.11	44.41	31.11	13.87	34.79
$\Delta G_{bind,\ PB}$	**−35.12**	**−35.94**	**−36.52**	**−41.22**	**−42.34**	**−42.25**
ΔG_{GB}	350.9	349.7	352.0	342.1	52.04	370.2
$\Delta G_{solv,GB}$	343.3	341.8	343.4	335.1	46.09	362.3
$\Delta G_{ele,\ GB}$	30.77	31.08	33.84	27.43	9.091	29.44
$\Delta G_{bind,\ GB}$	**−42.85**	**−46.00**	**−49.64**	**−47.02**	**−48.27**	**−47.42**

Bold values represent the ΔG_{bind} energy of molecules with tubulin based on MM-PBSA and MM-GBSA methods

reaction scheme is included in Fig. 4. The 9-bromonoscapine was prepared from natural α-noscapine using the synthetic scheme reported previously [19]. The complete chemical synthetic procedures for the preparation of noscapine derivatives, **5a–5f** and their characterization using ^{1}H, ^{13}C NMR and mass (ESI and HRMS), IR spectral data is described elsewhere. Further single crystal X-ray analysis unambiguously confirmed the structure of **5b** (Fig. 12). All

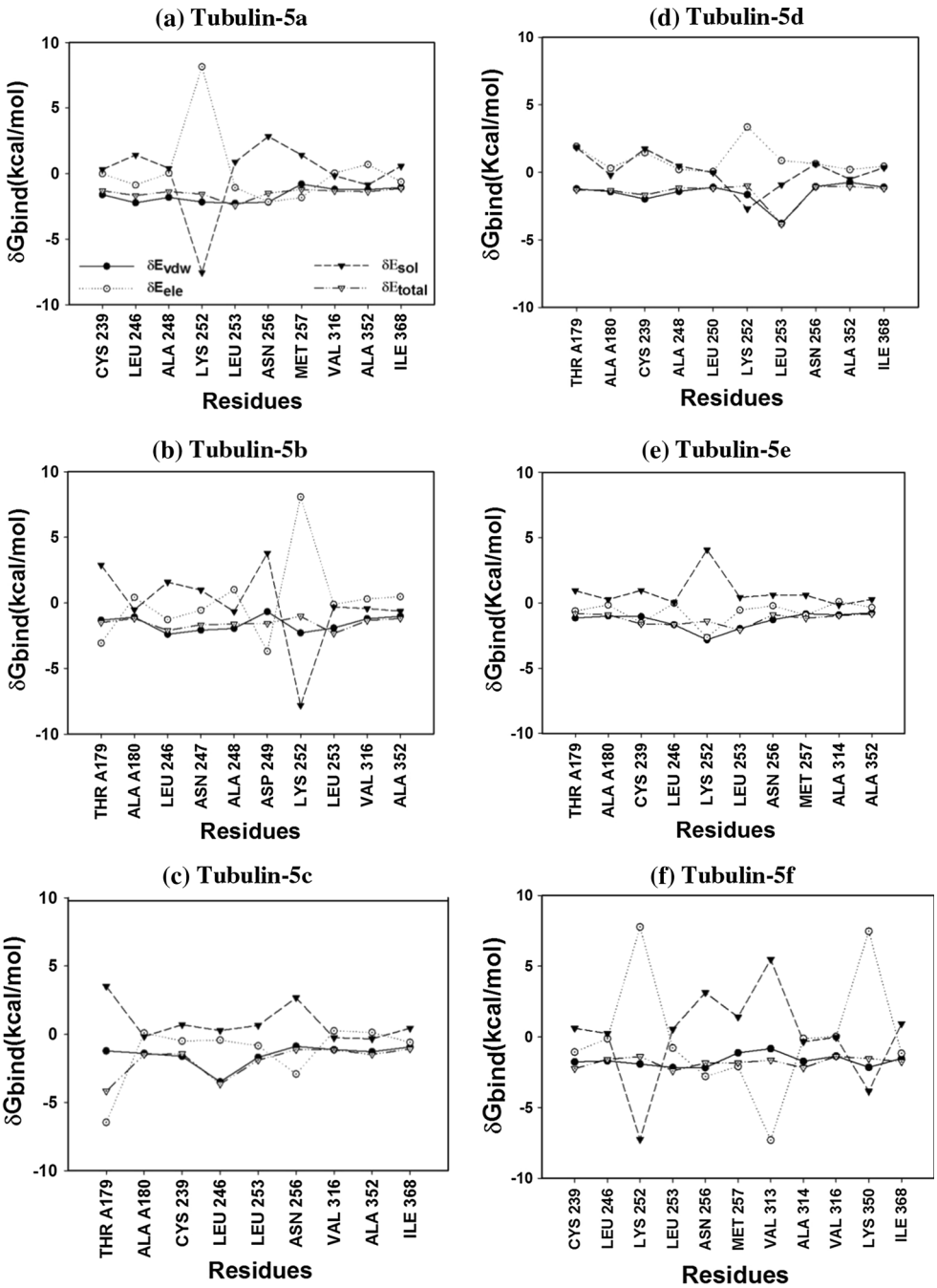

Fig. 11 Decomposition of the total binding energy (δG_{bind}) contribution of amino acids within and around binding site (12 Å of the docked ligand) of tubulin involved in interaction with noscapinoids **5a**–**5f** into several components such as: electrostatic (δE_{ele}), van der Waals (δE_{vdw}) and solvation (δE_{sol}) and per residue basis of the key residues (contributing $\delta G_{bind} < -1.0$ kcal/mol) in tubulin-drug complexes

the derivatives **5a**–**5f** were purified over silica gel column chromatography and used for experimental studies.

Biology

Newly designed noscapinoids have higher tubulin binding activity than noscapine

We first determined if all of the newly designed noscapine analogues bind tubulin in a manner similar to the founding compound, noscapine. We found that the newly designed noscapinoids **5a**–**5f** reduced the intrinsic fluorescence of tubulin in a concentration-dependent manner (Fig. 13) indicating concentration-dependent binding to tubulin. A plot of the inverse of fractional occupancy versus inverse of drug concentration yielded a dissociation constant (K_d) of 126 ± 5.0 μM for **5a**, 107 ± 5.0 μM for **5c**, 70 ± 4.0 μM for **5d**, and 68 ± 6.0 μM for **5e** binding to tubulin. We have previously reported the dissociation constant (K_d) of 152 ± 1.0 μM for noscapine binding to tubulin [19]. The results indicate that the newly designed noscapine analogues bind to tubulin with a greater affinity than

Table 4 Molecular docking results (Glide XP) as well as calculated energies based on LIE–SGB model of training set noscapine derivatives: van der Waals (vdw), electrostatic (elec), cavity (cav), predicted and experimental binding free energy (ΔG_{bind})

Ligand	Glide XP_{score} (kcal/mol)	$\langle U_{vdw} \rangle$ (kcal/mol)	$\langle U_{elec} \rangle$ (kcal/mol)	$\langle U_{cav} \rangle$ (kcal/mol)	K_d value (μM)	Experimental ΔG_{bind} (kcal/mol)	Predicted ΔG_{bind} (kcal/mol)
1	−5.505	−52.06	43.32	1.720	152 ± 1.0	−5.214	−5.194
2a	−5.684	−47.65	119.8	1.432	81 ± 8.0	−5.587	−5.951
2b	−6.152	−59.54	68.27	2.12	40 ± 8.0	−6.006	−6.063
2c	−6.437	−58.92	87.54	1.59	54 ± 9.1	−5.827	−6.355
2d	−5.463	−58.13	83.35	1.059	22 ± 4.0	−6.360	−5.755
2e	−6.228	−57.71	129.2	1.846	86 ± 6.0	−5.551	−5.835
2f	−5.279	−59.48	63.57	1.324	14 ± 1.0	−6.628	−6.540
3	−5.639	−53.28	87.36	0.823	68 ± 0.7	−5.691	−5.416
4a	−6.087	−63.42	41.26	0.824	91 ± 8.0	−5.518	−5.394
4b	−7.252	−62.62	76.32	1.232	38 ± 4.0	−6.036	−5.795
4c	−5.712	−61.82	41.32	0.698	79 ± 8.0	−5.602	−5.128
4d	−5.402	−56.95	7.851	0.756	228 ± 10.0	−4.973	−5.078

$\langle U_{vdw} \rangle$, $\langle U_{elec} \rangle$ and $\langle U_{cav} \rangle$ energy terms represents the ensemble average energy terms calculated as the difference between bound and free state of the ligands and its environment. Experimental ΔG_{bind} was calculated from the dissociation constant (K_d value) using the relationship: $\Delta G_{bind} = RT \ln K_d$ where T = 298 K and R = 0.00199 (kcal/mol K). Predicted ΔG_{bind} was calculated using (LIE–SGB empirical equation: $\Delta G_{bind} = 0.0762\langle U_{vdw} \rangle - 0.00965\langle U_{elec} \rangle - 0.520\langle U_{cav} \rangle$

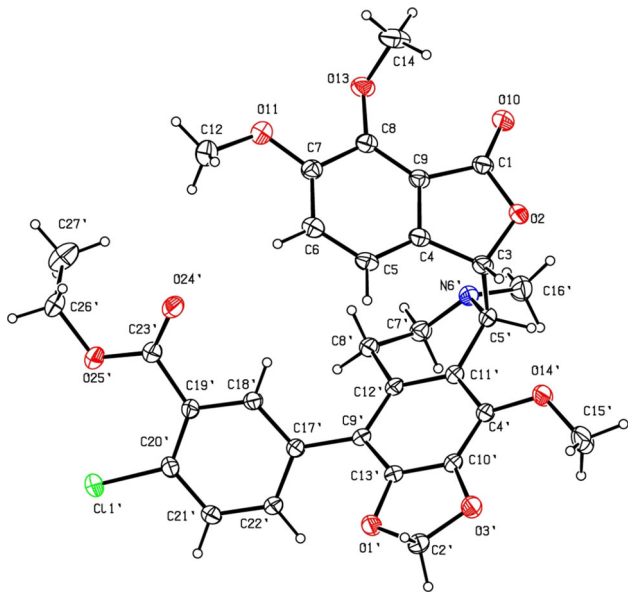

Fig. 12 A view of **5b**, showing the atom-labelling scheme. Displacement ellipsoids are drawn at the 30 % probability level and H atoms are represented by *circles* of arbitrary radii

noscapine. With the other two derivatives, **5b** and **5f,** although we observed quenching of intrinsic tryptophan fluorescence, the quenching pattern was not concentration-dependent. Therefore, we could not determine the dissociation constant for these two noscapinoids. Nevertheless, the quenching in the presence of both **5b** and **5f** indicate potential binding of these noscapinoids to tubulin (Fig. 13). Experimental $\Delta G_{bind,expt}$ of these compounds was calculated from the K_d value using the relationship: $\Delta G_{bind,expt} = RT \ln K_d$ where T = 298 K and R = 0.00199 (kcal/mol K). In fact, this experimentally determined values ($\Delta G_{bind,expt}$) are consistent with the predicted ($\Delta G_{bind,pred}$) values calculated using LIE–SGB (Tables 2, 4).

Newly designed noscapinoids inhibits proliferation of cancer cells

Based on the in vitro results, we analyzed the effectiveness of analogues **5a–5f** in inhibiting the proliferation of cancer cells. As a preliminary screen, all compounds, including the parent molecule, noscapine were evaluated for their anti-proliferative activity in three human cancer cell lines; human breast cancer cells (MCF-7), human cervical cancer cells (HeLa) and human lung adenocarcinoma cells (A549). The IC_{50} values for the test compounds **5a–5f** for these three cell lines are collated in Table 5. All the compounds exhibited improved cytotoxic activity in comparison to the founding compound, noscapine. Especially, three compounds **5b, 5e** and **5f** possess potent cytotoxic activity. The IC_{50} value amounted to 9.0 ± 1.5, 8.9 ± 1.7 and 9.2 ± 1.4 μM with **5b, 5e** and **5f** respectively for HeLa cells, which reflects a pronounced anti-proliferative activity. A similar low IC_{50} value of 18.8 ± 2.7, 16.6 ± 2.9 and 17.8 ± 2.5 μM was measured using **5b, 5e** and **5f** respectively for the MCF-7 cells. In contrast, modest anti-proliferative activity for these compounds was noted against A549 cell line. Thus this preliminary screen with the three chosen cell lines revealed that **5b, 5e** and **5f** as potent cytotoxic compounds as exemplified by their much lower IC_{50} values compared to noscapine.

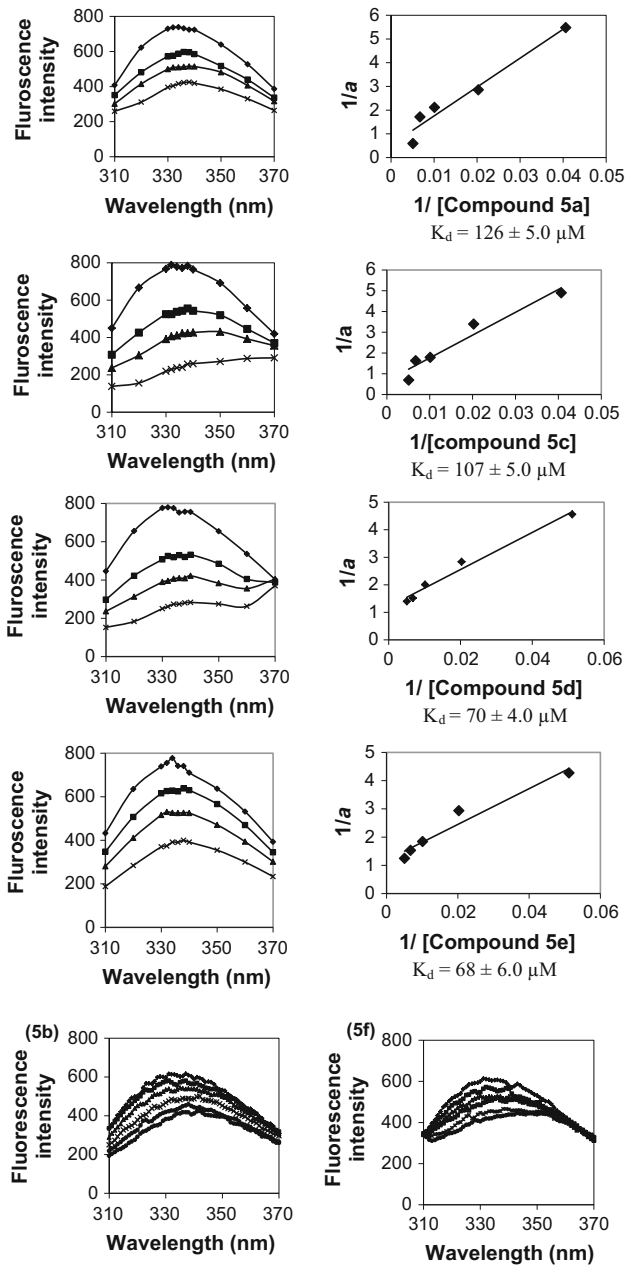

Fig. 13 *Plots* show concentration-dependent quenching of tubulin fluorescence emission intensity by noscapinoids **5a**–**5f**. The equilibrium dissociation constants (K_d) were determined from a plot of the inverse of fractional occupancy versus inverse of drug concentration

Newly designed noscapinoids alter the cell cycle profile and cause mitotic arrest at G_2/M phase

To ascertain the precise mechanisms of cell death, we next examined the effect of representative derivatives of noscapine **5a**–**5f** on the cell cycle progression of MCF-7 cells using a fluorescence activated cell sorting (FACS) analysis. We determined the effect of these compounds at 25 μM for 0, 24, 48 and 72 h of drug treatment. Figure 14a–d represents the cell cycle profile in a three-dimensional disposition for compounds **5b**–**5f** as cell cycle profile for **5a** is not shown in the figure (although data are already collected in Table 6). G_1 phase of the cell cycle represents the unreplicated cells with 2 N DNA, while G_2 and M phases represent the duplicated cells with 4 N DNA. Cells in the process of DNA duplication between 2 and 4 N peaks represent S phase, when DNA is being synthesized. Less than 2 N DNA appears in populations of dying cells that degrade their DNA to different extents. MCF-7 cells treated with these compounds for 0, 24, 48 and 72 h led to profound perturbations of the cell cycle profile at 25 μM (Fig. 14a–d). Our result reveals that these derivatives of noscapine induce a massive accumulation of cells in the G_2/M phase at 24 h. For example, the G_2/M cell population increases from 18.8 % in the control to ~58.7 % in MCF-7 cells treated with 25 μM of **5e** for 24 h. The distribution of cell populations over G_0/G_1, S, G_2/M and sub-G_1 phases of the cell cycle treated with 25 μM solution of noscapine derivatives is included in Table 6. Apropos to the G_2/M block, a characteristic hypodiploid DNA content (sub-G_1) was seen to be rising at 48 and 72 h of drug treatment. The progressive increase of cells having hypodiploid DNA content (Table 6) reflects fragmented DNA, indicating dying cells.

Table 5 IC_{50} values (a drug concentration required to achieve a 50 % inhibition of cellular proliferation) of noscapine derivatives **5a**–**5f** for various cancer cell types

Noscapine analogue	HeLa (μM)	A549 (μM)	MCF-7 (μM)
5a	22.8 ± 2.8	57.3 ± 3.9	41.3 ± 2.4
5b	9.0 ± 1.5	33.8 ± 3.5	18.8 ± 2.7
5c	21.2 ± 3.7	53.1 ± 3.7	40.7 ± 3.3
5d	20.3 ± 2.5	42.7 ± 2.9	34.3 ± 2.5
5e	8.9 ± 1.7	31.6 ± 2.6	16.6 ± 2.9
5f	9.2 ± 1.4	32.6 ± 2.5	17.8 ± 2.5
Noscapine	24.0 ± 2.9	62.9 ± 4.6	42.3 ± 2.7

Cancer cells used in the assay namely, *HeLa* human cervix cell line, *A549* human lung adenocarcinoma epithelial cell line and *MCF7*: human breast epithelial cell line

Each value represents mean ± SD from three different experiments

*Noscapinoid **5e** causes no detectable toxicity to tissues and does not affect the hematopoietic system and organ functions*

Toxicity in many tissues following chemotherapy is a major concern. Therefore, the search for a safe, well-tolerated regimen has been a major goal of anticancer research. Antimitotic drugs that bind free or polymerized tubulin, such as *Vinca* alkaloids and taxanes, although are effective treatment agents, are known to be cytotoxic to

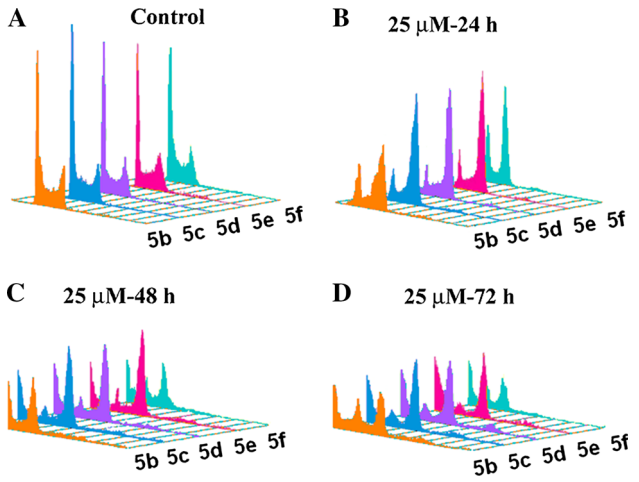

Fig. 14 Noscapine analogs inhibit cell cycle progression at mitosis followed by the appearance of a characteristic hypodiploid (sub-G1) DNA peak, indicative of apoptosis. **a**–**d** depict represented figures of analyses of cell cycle distribution in a three-dimensional disposition as determined by flow cytometry in MCF-7 cells treated with 25 μM concentration of noscapine analogs (**5b**–**5f**) for 0, 24, 58 and 72 h respectively

normal dividing cells. These drugs thus exhibit toxicities such as gastrointestinal (diarrhea, nausea, vomiting), myelosuppression (leucopenia), alopecia and peripheral neuropathies due to the blockage of axonal transport. To determine whether compound **5e** treatment results in toxicities to normal tissues, we did histopathologic analyses of vital organs such as liver, kidney, spleen, lung, heart, brain and duodenum of mice (Fig. 15). Treatment with compound **5e** daily at a dose of 300 mg/kg body weight for 28 days failed to reveal any detectable pathological abnormalities in normal tissues as examined by H&E staining. Similarly, in a different experiment, mice treated with a single dose of 600 mg/kg body weight also did not indicate any detectable pathological abnormalities. Paraffin-embedded 5 μ-thick sections of the liver, kidney, spleen, lung, heart, duodenum and brain from animals of both treated and normal group were examined by H&E staining and included in Fig. 15. There was a complete absence of any metastatic lesions in these organs in the treated animals. The liver showed normal hepatic lobular architecture. The kidneys revealed normal glomeruli, proximal and distal tubules, interstitium and blood vessels. The splenic follicles and vascular sinusoids were indistinguishable between the **5e**-treated and vehicle-treated control groups. The lung tissue showed normal alveoli and the heart muscle showed normal morphology among the two groups. Microsections of the brain did not reveal any infracted areas. The cerebral cortex, gray and white matter appeared normal. The gut showed normal mucosa, submucosa and muscularis mucosa.

Currently available anticancer drugs are known to depress bone marrow function, leading to decline of RBC, WBC and platelet counts during treatment regimens. Thus, we next examined if **5e** treatment had any effects on hematologic variables and organ-associated toxicities. Peripheral blood was examined for differences between **5e**-treated and vehicle-treated groups for complete blood count, white blood cell count, monocytes, eosinophils, red blood cell count, hemoglobin concentration, hematocrit, mean corpuscular volume, mean corpuscular hemoglobin, mean corpuscular haemoglobin concentration, and platelet count (Fig. 16a, b). We next assessed organ-associated toxicity by measuring organ functions in **5e**-treated and vehicle-treated groups. Liver function tests (alanine transaminase, aspartate aminotransferase, alkaline phosphatase, bilirubin levels and albumin levels) and renal function tests (blood urea nitrogen and creatinine levels) were similar between treated and control groups (Fig. 16c, d). Furthermore, **5e** does not alter the electrolyte balances. A standard electrolyte panel (Na^+, K^+, Cl^-, Ca) showed no abnormalities in electrolytes among the treated and control groups (Fig. 16e). In addition, we were surprised to find no changes among the treated and vehicle-treated groups in total protein, albumin and glucose levels (Fig. 16d, e).

Table 6 Effect of noscapine derivatives on cell cycle progression of MCF-7 cells treated with 25 μM solution for the indicated time (h) before being stained with propidium iodide for cell cycle analysis

	Cell cycle parameters (%)															
	0 h				24 h				48 h				72 h			
	Sub-G_1	G_0/G_1	S	G_2/M	Sub-G_1	G_0/G_1	S	G_2/M	Sub-G_1	G_0/G_1	S	G_2/M	Sub-G_1	G_0/G_1	S	G_2/M
5a	0.32	64.3	15.7	24.5	8.42	16.28	4.26	42.5	27.4	16.3	3.24	24.6	29.3	18.5	5.16	19.6
5b	0.28	56.8	13.5	22.7	12.2	15.8	4.19	52.4	31.7	14.2	4.28	38.2	36.4	10.6	7.28	29.3
5c	0.24	53.6	14.6	23.4	11.3	19.4	3.83	41.9	28.8	22.4	5.28	22.2	31.3	21.5	9.04	21.7
5d	0.18	68.4	12.3	19.3	7.43	14.3	3.77	65.2	36.5	6.47	3.29	44.6	47.5	7.25	4.08	35.6
5e	0.15	69.6	9.26	18.8	13.7	17.4	4.18	58.7	38.1	8.16	3.42	43.4	49.3	6.18	3.62	36.7
5f	0.17	55.3	14.6	21.4	9.37	12.5	3.58	56.2	35.8	7.15	3.08	49.8	50.2	4.39	2.63	32.4

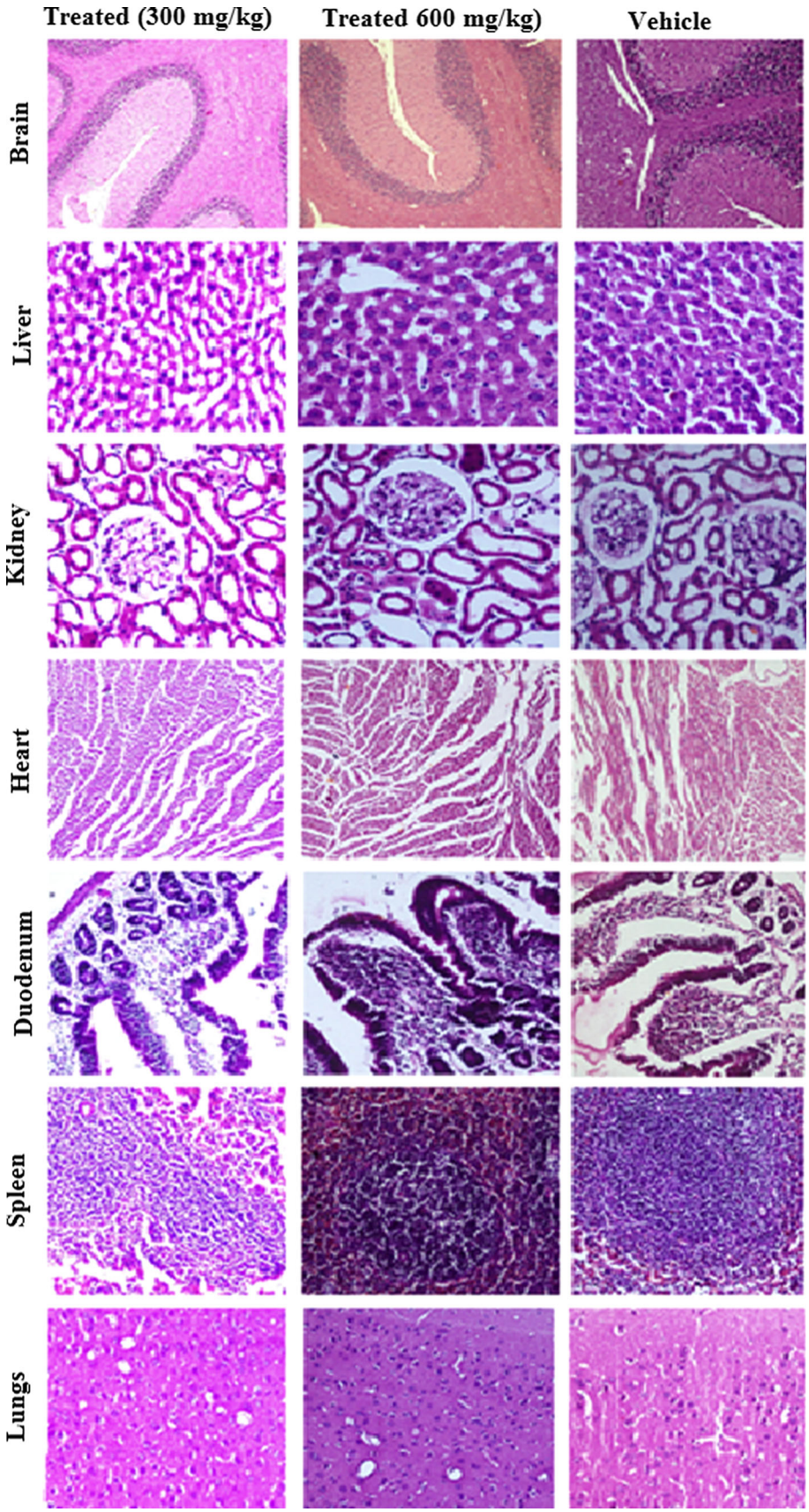

Fig. 15 Treated animals (both male and female) with **5e** and vehicle fails to reveal any detectable pathologic abnormalities in normal tissues that are active in normal cell proliferation. *Panels* represent H&E staining of paraffin-embedded 5 μ-thick sections of the liver, kidney, spleen, lung, heart, duodenum and brain from **5e**-treated and untreated groups of mice under ×200 magnifications. The liver showed normal hepatic lobular architecture. The kidneys revealed normal glomeruli, proximal and distal tubules, interstitium, and blood vessels. The splenic follicles and vascular sinusoids were indistinguishable between the **5e**-treated and vehicle-treated groups. The lung tissue showed normal alveoli and the heart muscle showed normal morphology among the two groups. Microsections of brain did not reveal any infracted areas. The cerebral cortex, *gray* and *white* matters appeared normal. The gut showed normal mucosa, submucosa and muscularis mucosa

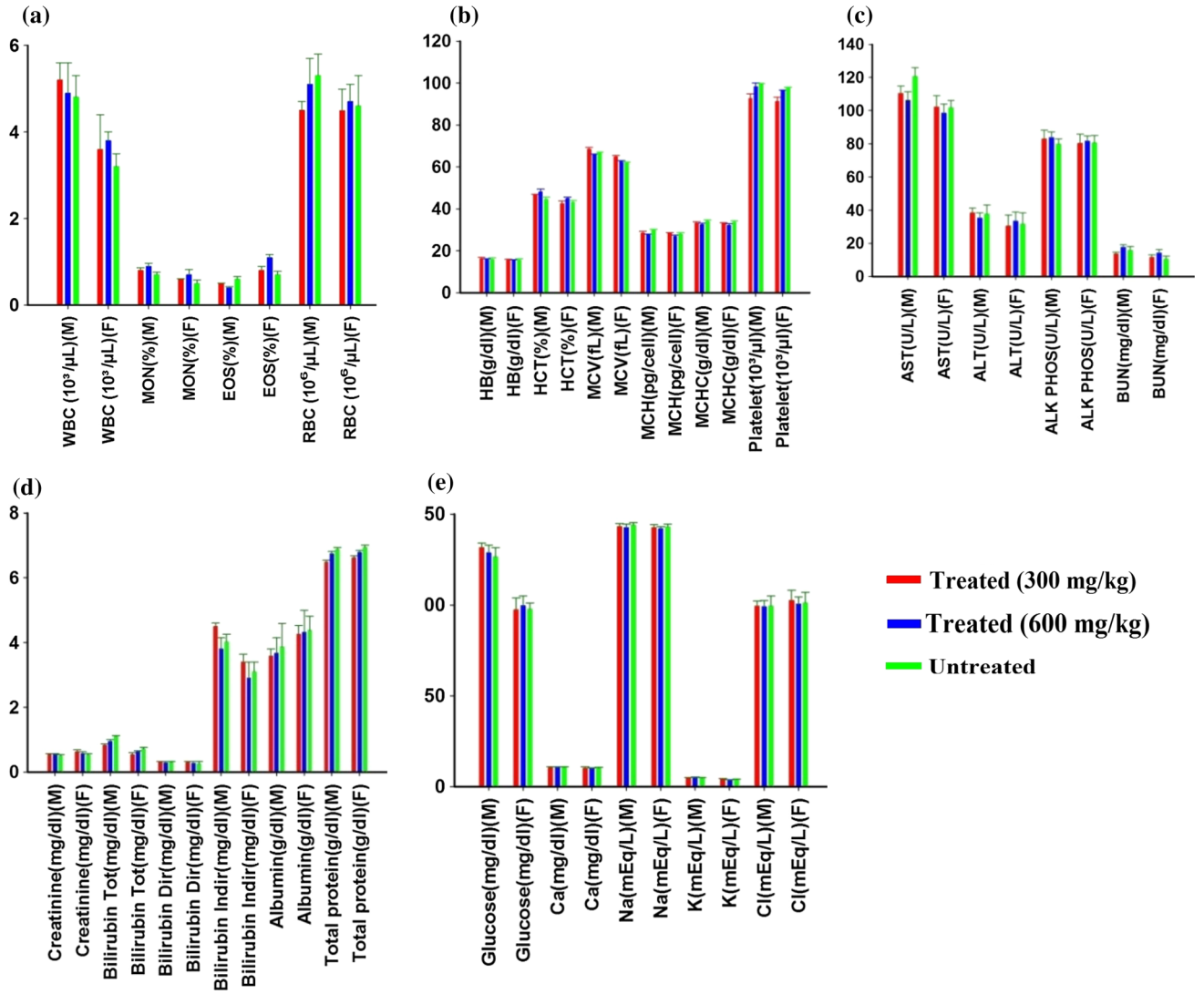

Fig. 16 Treated animals (both male and female) with **5e** show no deviation in the toxicity profile when compared with vehicle-treated controls. Figure shows no toxicities related to hematological variables (**a**, **b**) WBC count (WBC), monocytes (MON), eosinophils (EOS), RBC count (RBC), hemoglobin concentration (HB), Hematocrit (HCT), mean corpuscular volume (MCV), mean corpuscular hemoglobin (MCH), mean corpuscular hemoglobin concentration (MCHC) and platelet count. Organ functions (**c**, **d**) liver function tests (alkaline transaminase (ALT), aspartate aminotransferase (AST), alkaline phosphatase (ALK phos), bilirubin levels and albulin levels), renal function tests (blood urea nitrogen (BUN) and creatinine levels). Electrolyte panels (**e**) Na^+, K^+, Cl^-, and Ca. All show undistinguishable profiles among all variables examined for vehicle-treated and **5e**-treated groups

Also, during the dosage regimen, no abnormal behavior regarding food and water consumption and body weights was observed.

Conclusion

Inspired by the improved binding affinity by computational methods for the designed derivatives, we have provided the simplest methods for the direct and regioselective synthetic strategies that provided a new series of products in high quantitative yields. Most importantly, our results show that biaryl inserted noscapine analogues have higher affinity to tubulin compared to the parent compound, and that the substitution impacted their therapeutic potential for a variety of cancer types. Furthermore, the mechanism of cell death caused by these analogues is preserved, such that, like noscapine, cell death was preceded by extensive mitotic arrest. In vivo toxicological evaluation of one of the compounds **5e** did not reveal any toxicity in the vital organs such as liver, kidney, spleen, lung, heart, brain and duodenum. In addition, there was no significant difference in hematological and blood biochemical parameters between the treated and untreated groups. Our data thus show compelling

evidence that these analogues possess considerable potential for further preclinical and clinical evaluation.

Acknowledgments We are thankful to Jaypee University of Information Technology, India, for providing student's fellowship to Seneha Santoshi. We thank Mr. Birendra Patel, Professor in English, for proof reading the manuscript. We are greatly indebted to the anonymous reviewers of this manuscript for their helpful suggestions.

References

1. Mitchison TJ, Kirschner M (1984) Dynamic instability of microtubule growth. Nature 312:237–242
2. Kirschner M, Mitchison TJ (1986) Beyond self-assembly: from microtubules to morphogenesis. Cell 45:329–342
3. Van Tellingen O, Sips JH, Beijnen JH, Bult A, Nooijen WJ (1992) Pharmacology, bio-analysis and pharmacokinetics of the vinca alkaloids and semi-synthetic derivatives. Anticancer Res 12:1699–1715
4. Rowinsky EK (1997) The development and clinical utility of the taxane class of antimicrotubule chemotherapy agents. Annu Rev Med 48:353–374
5. Crown J, O'Leary M (2000) The taxanes: an update. Lancet 355:1176–1178
6. Goncalves A, Braguer D, Kamath K, Martello L, Briand C, Horwitz S, Wilson L, Jordan MA (2001) Resistance to taxol in lung cancer cells associated with increased microtubule dynamics. Proc Natl Acad Sci USA 98:11737–11741
7. Ye K, Ke Y, Keshava N, Shanks J, Kapp JA, Tekmal RR, Petros J, Joshi HC (1998) Opium alkaloid noscapine is an antitumor agent that arrests metaphase and induces apoptosis in dividing cells. Proc Natl Acad Sci USA 95:1601–1606
8. Ye K, Zhou J, Landen JW, Bradbury EM, Joshi HC (2001) Sustained activation of p34 (cdc2) is required for noscapine-induced apoptosis. J Biol Chem 276:46697–46700
9. Zhou J, Panda D, Landen JW, Wilson L, Joshi HC (2002) Minor alteration of microtubule dynamics causes loss of tension across kinetochore pairs and activates the spindle checkpoint. J Biol Chem 277:17200–17208
10. Zhou J, Gupta K, Yao J, Ye K, Panda D, Giannakakou P, Joshi HC (2002) Paclitaxel-resistant human ovarian cancer cells undergo c-Jun NH_2-terminal kinase-mediated apoptosis in response to noscapine. J Biol Chem 277:39777–39785
11. Ke Y, Ye K, Grossniklaus HE, Archer DR, Joshi HC, Kapp JA (2000) Noscapine inhibits tumor growth with little toxicity to normal tissues or inhibition of immune responses. Cancer Immunol Immunother 49:217–225
12. Landen JW, Lang R, McMahon SJ, Rusan NM, Yvon AM, Adams AW, Sorcinelli MD, Campbell R, Bonaccorsi P, Ansel JC, Archer DR, Wadsworth P, Armstrong CA, Joshi HC (2002) Noscapine alters microtubule dynamics in living cells and inhibits the progression of melanoma. Cancer Res 62:4109–4114
13. Landen JW, Hau V, Wang MS, Davis T, Ciliax B, Wainer BH, Van Meir EG, Glass JD, Joshi HC, Archer DR (2004) Noscapine crosses the blood-brain barrier and inhibits glioblastoma growth. Clin Cancer Res 10:5187–5201
14. Dahlstrom B, Mellstrand T, Lofdahl C, Johansson M (1982) Pharmacokinetic properties of noscapine. Eur J Clin Pharmacol 22:535–539
15. Segal MS, Goldstein MM, Attinger EO (1957) The use of noscapine (narcotine) as an antitussive agent. Dis Chest 32:305–309
16. Loder RE (1969) Safe reduction of the cough reflex with noscapine: a preliminary communication on a new use for an old drug. Anaesthesia 24:355–358
17. Santoshi S, Naik PK, Joshi HC (2011) Rational design of novel anti-microtubule agent (9-azido-Noscapine) from quantitative structure activity relationship (QSAR) evaluation of noscapinoids. J Biomol Screen 16:1047–1058
18. Naik PK, Chatterji BP, Vangapandu SN, Aneja R, Chandra R, Kanteveri S, Joshi HC (2011) Rational design, synthesis and biological evaluations of amino-noscapine: a high affinity tubulin-binding noscapinoid. J Comput Aided Mol Des 25:443–454
19. Naik PK, Lopus M, Aneja R, Vangapandu SN, Joshi HC (2012) In silico inspired design and synthesis of a novel tubulin-binding anti-cancer drug: folate conjugated noscapine (Targetin). J Comput Aided Mol Des 26:233–247
20. Manchukonda NK, Naik PK, Santoshi S, Lopus M, Joseph S, Sridhar B, Kantevari S (2013) Rational design, synthesis and biological evaluation of third generation α-noscapine analogues as potent tubulin binding anti-cancer agents. PLoS One 8(10):e77970
21. Jain N, Yada D, Shaik TB, Vasantha G, Reddy PS, Kalivendi SV, Sreedhar B (2011) Synthesis and antitumor evaluation of nitrovinyl biaryls: anticancer agents based on allocolchicines. Chem Med Chem 6(5):859–868
22. Marzaro G, Coluccia A, Ferrarese A, Brun P, Castagliuolo I, Conconi MT, Regina GL, Bai R, Silvestri R, Hamel E, Chilin A (2014) J Med Chem 57:4598–4605
23. Lee C, Yang W, Parr RG (1988) Development of the Colle-Salvetti correlation-energy formula into a functional of the electron density. Phys Rev B 37:785–789
24. Becke AD (1993) A new mixing of Hartree–Fock and local density-functional theories. J Chem Phys 98:1372–1377
25. Gordon MS, Binkley JS, Pople JA, Pietro WJ, Hehre WJ (1982) Self-consistent molecular-orbital methods. 22. Small split-valence basis sets for second-row elements. J Am Chem Soc 104:2797–2803
26. Berendsen HJC, van der Spoel D, van Drunen R (1995) GROMACS: a message passing parallel molecular dynamics implementation. Comput Phys Commun 91:43–56
27. Laskowski RA, Moss DS, MacArthur MW, Thornton JM (1993) PROCHECK: a program to check the stereochemical quality of protein structures. J Appl Crystal 26:283–291
28. Colovos C, Yeates TO (1993) Verification of protein structures: patterns of non-bonded atomic interactions. Protein Sci 2:1511–1519
29. Eisenberg D, Luthy R, Bowie JU (1997) VERIFY3D: assessment 694 of protein models with three-dimensional profiles. Methods Enzymol 277:396–404
30. Ramachandran GN, Ramakrishnan C, Sasisekharan V (1963) Stereochemistry of polypeptide chain configurations. J Mol Biol 7:95–99
31. Naik PK, Santoshi S, Rai A, Joshi HC (2011) Molecular modelling and competition binding study of Br-noscapine and colchicine provide insight into noscapinoid-tubulin binding site. J Mol Graph Model 29:947–955
32. Friesner RA, Banks JL, Murphy RB, Halgren TA, Klicic JJ, Mainz DT, Repasky MP, Knoll EH, Shelley M, Perry JK, Shaw DE, Francis P, Shenkin PS (2004) Glide: a new approach for rapid, accurate docking and scoring. 1. Method and assessment of docking accuracy. J Med Chem 47:1739–1749
33. Halgren TA, Murphy RB, Friesner RA, Beard HS, Frye LL, Pollard WT, Banks JL (2004) Glide: a new approach for rapid, accurate docking and scoring. 2. Enrichment factors in database screening. J Med Chem 47:1750–1759
34. Case DA, Darden TA, Cheatham TE, Simmerling CL, Wang J, Duke RE, Luo R, Walker RC, Zhang W, Merz KM, Roberts B, Wang B, Hayik S, Roitberg A, Seabra G, Kolossváry I, Wong KF, Paesani F, Vanicek J, Liu J, Wu X, Brozell SR, Steinbrecher T, Gohlke H, Cai Q, Ye X, Wang J, Hsieh MJ, Cui G, Roe DR,

Mathews DH, Seetin MG, Sagui C, Babin V, Luchko T, Gusarov S, Kovalenko A, Kollman PA (2010) AMBER 11. University of California, San Francisco
35. Cornell WD, Cieplak P, Bayly CI, Gould IR, Merz KM Jr, Ferguson DM, Spellmeyer DC, Fox T, Caldwell JW, Kollman PA (1995) A second generation force field for the simulation of proteins, nucleic acids, and organic molecules. J Am Chem Soc 117:5179–5197
36. Ryckaert JP, Ciccotti G, Berendsen HJC (1977) Numerical integration of the Cartesian equations of motion of a system with constraints: molecular dynamics of n-alkanes. J Comput Phys 23:327–341
37. Daren T, York D, Pedersen L (1993) Particle mesh Ewald: an N-log(N) method for Ewald sums in large systems. J Chem Phys 98:10089–10092
38. Hornak V, Abel R, Okur A, Strockbine B, Roitberg A, Simmerling C (2006) Comparison of multiple Amber force fields and development of improved protein backbone parameters. Protein 65:712–725
39. Berendsen HJC, Postma JPM, Van Gunsteren WF, DiNola A, Haak JR (1984) Molecular dynamics with coupling to an external bath. J Chem Phys 81:3684–3691
40. Srinivasan J, Cheatham TE, Cieplak P, Kollman PA, David A (1998) Case continuum solvent studies of the stability of DNA, RNA, and phosphoramidate-DNA helicesm. J Am Chem Soc 120:9401–9409
41. Kollman PA, Massova I, Reyes C, Kuhn B, Huo S, Chong L, Lee M, Lee T, Duan Y, Wang W, Donini O, Cieplak P, Srinivasan J, Case DA, Cheatham TE (2000) Calculating structures and free energies of complex molecules: combining molecular mechanics and continuum models. Acc Chem Res 33:889–897
42. Zhou R, Frienser RA, Ghosh A, Rizzo RC, Jorgensen WL, Levy RM (2001) New linear interaction method for binding affinity calculations using a continuum solvent model. J Phys Chem B 105:10388–10397
43. Aneja R, Vangapandu SN, Lopus M, Viswesarappa VG, Dhiman N, Verma A, Chandra R, Panda D, Joshi HC (2006) Synthesis of microtubule-interfering halogenated noscapine analogues that perturb mitosis in cancer cells followed by cell death. Biochem Pharmacol 72:415–426
44. Aneja R, Vangapandu SN, Lopus M, Chandra R, Panda D, Joshi HC (2006) Development of a novel nitro-derivative of noscapine for the potential treatment of drug-resistant ovarian cancer and Tcell lymphoma. Mol Pharmacol 69:1801–1809
45. Bruker (2001) SAINT (version 6.28a) and SMART (version 5.625). Bruker AXS Inc., Madison, Wisconsin
46. Sheldrick GM (2008) A short history of SHELX. Acta Crystallogr A64:112–122
47. Flack HD, Bernardinelli G (2000) Reporting and evaluating absolute-structure and absolute-configuration determinations. J Appl Crystallogr 33:1143–1148
48. Hamel E, Lin CM (1981) Glutamate-induced polymerization of tubulin: characteristics of the reaction and application to the large-scale purification of tubulin. Arch Biochem Biophys 209:29–40
49. Panda D, Chakrabarti G, Hudson J, Pigg K, Miller HP, Wilson L, Himes RH (2000) Suppression of microtubule dynamic instability and treadmilling by deuterium oxide. Biochemistry 39:5075–5081
50. Bradford MM (1976) A rapid and sensitive method for the quantitation of microgram quantities of protein utilizing the principle of protein/dye binding. Anal Biochem 72:248–254
51. Zhou J, Gupta K, Aggarwal S, Aneja R, Chandra R, Panda D, Joshi HC (2003) Brominated derivatives of noscapine are potent microtubule-interfering agents that perturb mitosis and inhibit cell proliferation. Mol Pharmacol 63:799–807
52. Aneja R, Dhiman N, Idnani J, Awasthi A, Arora SK, Chandra R, Joshi HC (2007) Preclinical pharmacokinetics and bioavailability of noscapine, a tubulin-binding anticancer agent. Cancer Chemother Pharmacol 60:831–839